Chapter 3: Numerical modelling for Single Phase Natural Circulation Loop using various working fluids

This chapter presents the one-dimensional steady-state and transient analyses for Vertical Heating Horizontal Cooling (VHHC) SPNCL with water, water-based binary and ternary nanofluids, and thermal oils as the working fluids. The parametric investigation includes the effect of geometrical parameters like tube diameter, loop height, loop aspect ratio (height to width), loop inclination, nanoparticle shapes, and power input on the SPNCL performance parameters such as mass flow rate, effectiveness of heat exchanger, and total entropy generation rate.

3.1 Methodology

In the present analysis, a rectangular VHHC-SPNCL has been considered, which consists of a heater, cooler, hot leg, and cold leg, as shown in Fig. 3.1. A constant heat flux boundary condition is applied at the heater, and the cooler is modeled as a counter-flow type heat exchanger for simplicity. The coolant temperature is kept constant throughout the cooling section by maintaining negligible temperature difference (less than $1^{o}C$) between coolant outlet and inlet temperature by supplying sufficiently high mass flow rate. The adiabatic boundary condition is applied to the hot leg and cold leg sections.

Water, water-based binary and ternary hybrid-nanofluids, and thermal oils are selected as the working or primary fluid in the loop, and water is used as the secondary fluid or as a coolant. It is noteworthy to mention that the Prandtl number for water and thermal oil, a heat transfer fluid for parabolic trough collector, differs significantly. The thermophysical properties of the working fluid are estimated at its average temperature over the entire loop. The coolant inlet temperature is set as the reference temperature for the described SPNCL.

The derived one-dimensional governing equations and the numerical approach are described subsequently.

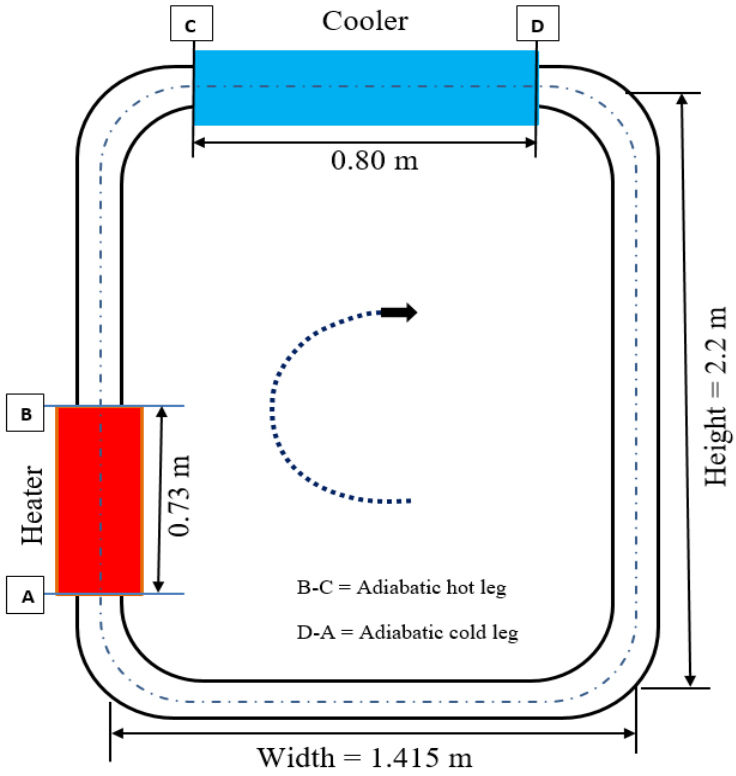

Fig. 3.1 Schematic of SPNCL with Vertical Heater Vertical Cooler arrangement

3.1.1 Governing Equations

The following assumptions are considered to derive one-dimensional governing equations:

(i) Fluid density is based on Boussinesq approximation, i.e. $\rho = \rho_0 \left[1 - \beta_{avg}\left(T - T_0\right)\right]$.

(ii) Viscous dissipation for working fluid has is neglected.

(iii) Heat losses are ignored considering insulated loop design.

(iv) The SPNCL is leak-proof.

The conservation of mass for the SPNCL is given by,

$$\frac{\partial \rho}{\partial t} + \frac{\partial \dot{m}}{A \partial s} = 0 \tag{3.1}$$

The conservation of momentum for the SPNCL is given by,

$$\frac{L_t}{A}\frac{\partial \dot{m}}{\partial t} = \rho_0 g \beta_{avg} \oint T \cos(\theta + \varphi) ds - (\frac{fL_t}{d} + K)\frac{\dot{m}^2}{2\rho_o A^2} \tag{3.2}$$

The conservation of energy for the SPNCL fluid is given by,

$$\rho c_p \frac{\partial T}{\partial t} + \frac{\dot{m} c_p \partial T}{A \partial s} - \frac{\partial^2 (kT)}{\partial s^2} = -\frac{h_i \xi_i (T - T_W)}{A} \tag{3.3}$$

Where θ is the flow direction and φ is the loop inclination with respect to the vertical axis. For the right vertical-leg θ = 0º, top horizontal-leg θ = 90º, left vertical-leg θ =180º and bottom horizontal-leg θ =270º. Therefore, the developed numerical tool is generic in nature and allows investigation of several arrangements of heater and cooler. However, in the present case, the focus is on the VHHC arrangement because this orientation shows the best performance considering both stability and induced mass flow rate [28]. A schematic of an inclined SPNCL is shown in Fig 3.2. The analysis of the inclination of VHHC loop can be useful for the nuclear power ship, where the pitching and rolling motion of the ship have a great influence on the natural circulation mass flow rate and stability.

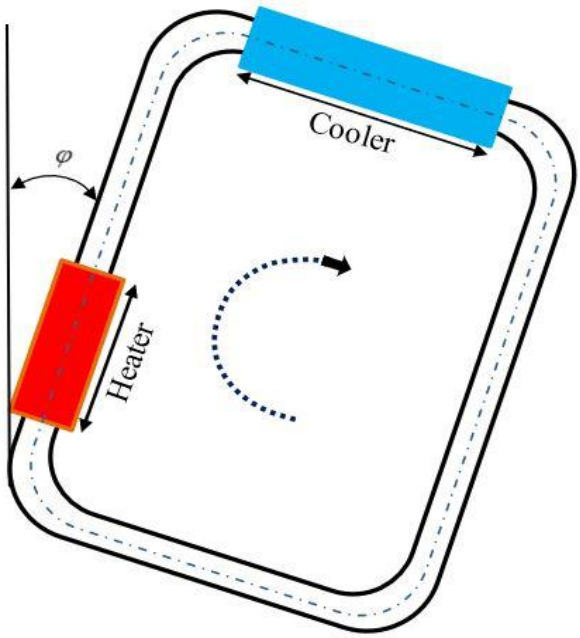

Fig. 3.2 A schematic of an inclined SPNCL

Energy conservation equation (per unit volume) for tube wall for different sections:

$$\rho_w c_{pw} \frac{\partial T_w}{\partial t} - \frac{\partial^2 (k_w T_w)}{\partial s^2} = -\frac{h_i \xi_i (T_w - T)}{A_w} + \frac{Q}{V_w} \quad \text{Heating section} \quad (3.4)$$

$$\rho_w c_{pw} \frac{\partial T_w}{\partial t} - \frac{\partial^2 (k_w T_w)}{\partial s^2} = -\frac{h_i \xi_i (T_w - T)}{A_w} \quad \text{Hot and cold leg} \quad (3.5)$$

$$\rho_w c_{pw} \frac{\partial T_w}{\partial t} - \frac{\partial^2 (k_w T_w)}{\partial s^2} = -\frac{h_i \xi_i (T_w - T)}{A_w} - \frac{h_S \xi_S (T_w - T_S)}{A_w} \quad \text{Heat exchanger} \quad (3.6)$$

Energy conservation equation for secondary (coolant) fluid in the heat exchanger:

$$\frac{\rho c_p \partial T_S}{\partial t} + \frac{\dot{m} c_p \partial T_S}{A_S \partial s} - \frac{\partial^2 k_S T_S}{\partial s^2} = \frac{h_S \xi_S (T_W - T_S)}{A_S} \quad (3.7)$$

Where Q is the heater power input; h_i and h_S are the heat transfer coefficients associated with the inner wall of the tube with the primary fluid and the outer wall of the tube with the secondary fluid; ξ_i and ξ_S are the inner and outer perimeters of the tube; V_w and A_w are the volume and the cross-sectional area of the tube wall, respectively.

3.1.2 Properties of the working fluids

The temperature-dependent thermophysical for the base fluids (Water and thermal oils) are obtained from the EES library. The properties of binary and ternary hybrid nanofluids like density, coefficient of thermal expansion, and specific heat depend on the volume concentration of nanoparticles and their individual properties (Table 3.1 [99-104]). Therefore, these properties are calculated by using the mixture model as follows [98]:

$$\rho_{hnf} = \sum_p \phi_p \rho_p + (1-\phi)\rho_f \quad (3.8)$$

$$(\rho\beta)_{hnf} = \sum_p \phi_p \rho_p \beta_p + (1-\phi)(\rho\beta)_f \quad (3.9)$$

$$(\rho c_p)_{hnf} = \sum_p \phi_p \rho_p c_{p,p} + (1-\phi)(\rho c_p)_f \quad (3.10)$$

Table 3.1 Some important numerical investigations on SPNCL [99-104].

Thermophysical property	Ag (Spherical)	Cu (Spherical)	Graphene (platelets)	Al_2O_3 (Spherical)	TiO_2 (Spherical)	CNT (Cylindrical)
$\rho(kg/m^3)$	10500	8933	2200	3970	4250	2100
$C_p(J/kgK)$	235	385	790	765	686.2	410
$k(W/mK)$	429	400	5000	40	8.9538	3007.4
$\beta(K^{-1})$	0.000054	0.000051	-0.000008	0.000024	0.000024	0.00002

The transport properties of binary and ternary hybrid nanofluids like thermal conductivity and dynamic viscosity depend on the volumetric concentration, their individual properties, and the shape (cylindrical, spherical and platelets) of nanoparticles. In this analysis, the influence of particle concentration and the nanoparticle shape has been considered. Thermal conductivity of *mono-dispersed nanofluid* having nanoparticles of different shapes are calculated with the Hamilton–Crosser model as follows:

$$\frac{k_{nf,p}}{k_f} = \frac{k_p + (n-1)k_f + (n-1)\phi(k_p - k_f)}{k_p + (n-1)k_f - \phi(k_p - k_f)} \tag{3.11}$$

where, $n = \frac{3}{\psi}$, n = empirical shape factor, ψ = Sphericity.

Likewise, the viscosity of mono nanofluid having nanoparticles of different shapes is given by [105],

$$\mu_{nf,p} = \mu_f(1 + B\phi + C\phi^2) \tag{3.12}$$

where B and C are viscosity enhancement coefficients. These are summarized in Table 3.2. Dynamic viscosity and thermal conductivity for *binary and ternary hybrid nanofluids* with

nanoparticles of different compositions and shapes have been calculated using an interpolation method. Hence, the effective dynamic viscosity and thermal conductivity of a hybrid nanofluid with different types of nanoparticles are calculated by,

$$\mu_{hnf} = \frac{1}{\phi}\sum_{p}\left(\phi_p \mu_{nf,p}\right) \text{ where } \phi = \sum_{p}\phi_p \tag{3.13}$$

$$k_{hnf} = \frac{1}{\phi}\sum_{p}\left(\phi_p k_{nf,p}\right) \tag{3.14}$$

where, ϕ_p, $\mu_{nf,p}$ and $k_{nf,p}$ are volume concentration of individual particle, dynamic viscosity (Eq. 3.11) and thermal conductivity (Eq. 3.10) of mono nanofluids, respectively. Where for binary hybrid nanofluid p=2, ternary hybrid nanofluid p=3.

Table 3.2 Sphericity, Empirical shape factor, and viscosity enhancement coefficient of different shapes of nanoparticles [105].

Nanoparticle shape	Sphericity (ψ)	Empirical shape factor (n)	B	C
Spherical	1	3	2.5	6.2
Cylindrical	0.6122	4.9	13.5	904.4
platelets	0.52	5.7	37.1	612.6

3.1.3 Nusselt number and friction factor

In the transient analysis, the local flow regime (laminar, transition or turbulent) depends on the loop geometry and input power. Therefore, a proper estimation of the friction factor and the heat transfer coefficient is necessary. For the friction factor, the suggested correlation by Swapnalee and Vijayan [75] for SPNCL is adopted. This is defined as the maximum of $f_{laminar}$, $f_{transition}$ and $f_{turbulent}$ for a smooth transition between laminar, transition

and turbulent regimes, wherever necessary. The friction factor correlations used for base fluid are given below:

$$f_{laminar} = 64/\mathrm{Re} \qquad \mathrm{Re} \le 898 \qquad (3.15)$$

$$f_{transition} = 1.2063/\mathrm{Re}^{0.416} \qquad 898 \le \mathrm{Re} \le 3196 \qquad (3.16)$$

$$f_{turbulent} = 0.316/\mathrm{Re}^{0.25} \qquad \mathrm{Re} \ge 3196 \qquad (3.17)$$

the friction factor for pure fluids is adopted for nanofluids, assuming its homogeneous nature. Indeed, there may be some limitations; however, considering the fact that pressure drop = f (Reynolds number and roughness) and nature of flow depends on Reynolds number, not affected by nanoparticles. Therefore, for now, safe to assume these correlations.

The total local loss coefficient (K in Eq. 2) of 3.6 is considered in this analysis due to four bends (0.9 each), as given by Vijayan [106].

Nusselt number correlations for different flow regimes are as follows:

Nusselt number correlations for water and thermal oils as the primary (working) fluid:

Laminar flow regime (Re≤2300) [107]:

$Nu = 1.86\,\mathrm{Re}^{1/3}\,\mathrm{Pr}^{1/3}(d/L_C)^{1/3}$ (developing flow, both cooling and heating, Gz>10) (3.18)

$Nu = 3.66$ (fully developed flow, Gz≤10, isothermal boundary condition) (3.19)

$Nu = 4.36$ (fully developed flow, Gz≤10, constant heat flux boundary condition) (3.20)

where, $Gz = (\pi d/4L_C)\,\mathrm{Re}\,\mathrm{Pr}$

Transition and turbulent flow regime [108]:

$$Nu = 0.012(\mathrm{Re}^{0.87} - 280)\,\mathrm{Pr}^{0.4} \qquad (3.21)$$

valid for $1.5 < \mathrm{Pr} < 500$, $3000 \le \mathrm{Re} \le 10^6$.

Nusselt number for binary and ternary hybrid-nanofluids as the primary (working) fluids:

Laminar flow regime [109]:

$$Nu_{hnf} = 2.03 Re_{hnf}^{0.293} \Pr_{hnf}^{0.6} \phi^{0.06} (d / L_c)^{0.37} \quad (3.22)$$

Applicable range: $Re_{hnf} < 2500$ and $0\% \leq \phi \leq 6\%$.

Transition and turbulent flow regimes [110]:

$$Nu_{hnf} = 0.065(Re_{hnf}^{0.65} - 60.22)(1 + 0.0169\phi^{0.15}) \Pr_{hnf}^{0.542} \quad (3.23)$$

valid for, 3000 < Re < 16,000 and 0< ϕ < 0.1, where, $\mathrm{Re}_{hnf} = \frac{\dot{m}_{hnf} d}{\mu_{hnf} A}$, $\Pr_{hnf} = \frac{\mu_{hnf} c_{phnf}}{k_{hnf}}$.

Nusselt number correlations for the secondary (coolant) fluid [107]:

Convective heat transfer coefficient for secondary fluid in the cooler is estimated by the following Nusselt number correlation for fully developed turbulent flow:

$$Nu = 0.023 \mathrm{Re}^{0.8} \Pr^{0.4} \quad (3.24)$$

3.1.4 Numerical scheme and performance parameters

The coupled ordinary differential equations (Eqs. 3.1 to Eq. 3.7) are solved using the finite difference method (FDM). The transient term in the energy and momentum equation is discretized by using the implicit, first-order, forward difference approximation. The first-order upwind discretization is used for the temperature convection term, and the second-order central difference is used for the diffusion term. The discretized equations have been solved by Engineering Equation Solver [111].

Three important performance parameters viz. Buoyancy force induced mass flow rate, Effectiveness of cooler and the total entropy generation rate is used for comparing the different working fluids. This provides the energy-exergy performance of the loop. The performance parameters are calculated by using given following equations;

a. ***Buoyancy force induced mass flow rate of the working fluid inside the loop***: it is obtained by solving the coupled governing equations (3.1-3.7), which predict the heat transport capability of the system.

b. Effectiveness is defined for the cooler: The ratio of actual heat transfer to the maximum possible heat transfer through the cooler. it predicts the heat transfer capability of the system as given by [52]. Therefore, for the better performance heat exchanger should have higher effectiveness.

$$\varepsilon = \frac{\dot{m}c_p(T_{C,in} - T_{C,out})}{(\dot{m}c_p)_{\min}(T_{C,in} - T_{S,in})} \tag{3.25}$$

a. ***The total entropy generation rate of the loop***: The entropy generation rate predicts the amount of irreversibility or wasted energy in the process of heat transfer and pressure drop. It is a measure of the thermodynamic inefficiency of the heat exchanger. The entropy generation rate for different heating, cooling and adiabatic section is given by equation 3.26, 3.27, and 3.28 respectively,

$$S_{gen,H} = \dot{m}\left[c_p \ln\left(\frac{T_{H,out}}{T_{H,in}}\right) + \frac{fL_H\dot{m}^2}{2d\rho_{H,avg}^2 A^2 T_{H,avg}} - \frac{c_p\left(T_{H,out} - T_{H,in}\right)}{T_{wall,H}}\right] \tag{3.26}$$

Entropy generation rate in heat exchanger is derived assuming constant and uniform coolant temperature condition. However, the entropy generation due to coolant pressure drop has been neglected.

$$S_{gen,C} = \dot{m}\left[c_p \ln\left(\frac{T_{C,out}}{T_{C,in}}\right) + \frac{fL_C\dot{m}^2}{2d\rho_{C,avg}^2 A^2 T_{C,avg}} - \frac{c_p\left(T_{C,out} - T_{C,in}\right)}{T_S}\right] \tag{3.27}$$

$$S_{gen,leg} = \frac{f\dot{m}^3}{2dA^2}\left[\frac{L_h}{\rho_{h,avg}^2 T_{h,avg}} + \frac{L_c}{\rho_{c,avg}^2 T_{c,avg}}\right] \tag{3.28}$$

Thus, the total entropy generation rate in the SPNCL is given by,

$$S_{gen,t} = S_{gen,H} + S_{gen,C} + S_{gen,leg} \tag{3.29}$$

The practical relevance of effectiveness and total entropy generation is that, for a given heat input the SPNCL having higher heat exchanger effectiveness will have higher temperature drop in the cooling section resulting lower heat exchanger outlet temperature, which reduces the maximum temperature of the of the fluid in the loop. The maximum

temperature of the fluid is fixed for single phase i.e., boiling point of the working fluid. Therefore, SPNCL having higher effectives can be used to transfer higher heat input without undergoing any phase change. Similarly, the entropy generation generates due to the irreversibility produced due to heat transfer and pressure drop which provides the quantitative measure of process inefficiency. The SPNCL having higher entropy generation means it has less capacity to transfer the heat from source to sink. Therefore, the performance parameter effectiveness, and total entropy generation rate can be useful for the selection of the heat transfer fluid and also for the design of natural circulation based heat exchangers for the better performance of the SPNCL system.

3.1.5 Grid and time-independent test

Grid and time independence tests have been performed to ensure (a) consistency of the obtained result and (b) the numerical error arising out of temporal discretization is minimized for the selected scheme. The computed mass flow rate for the three grid sizes (0.01m, 0.03m and 0.06m) and four time-steps (1s, 0.5s, 0.1s and 0.05s) are shown in Figs. 3.3a and Fig. 3.3b, respectively, for an input power of 500 W. The analyses provide an optimal grid size of 0.03 m and a time-step of 0.1s, which are maintained for further investigations. Also, the Grid Convergence Index (GCI) has been calculated by using the Roache method [112] for mass flow rate at 500 W power input to calculate the discretization error shown in Table 3.3.

Table 3.3 Calculation of discretization error.

∅= Mass flow rate at 500 W power input					
		Fine Grid Sets (N_1 and N_2)		Coarse Grid Sets (N_2 and N_3)	
N_1, N_2, N_3	723, 241, 121	$\emptyset_{ext}^{21}$	0.0283	$\emptyset_{ext}^{32}$	0.0283
	3	e_a^{21}	0.78%	e_a^{32}	1.1%
r_{32}	2	e_{ext}^{21}	0.5%	e_{ext}^{32}	1.22%

$\emptyset_1$	0.02842	GCI_{fine}^{21}	0.55%	GCI_{fine}^{32}	1.51%
$\emptyset_2$	0.02864				
$\emptyset_3$	0.02895				
p	0.9255				

Where, $p=\frac{1}{\ln(r_{21})}|ln|\epsilon_{32}/\epsilon_{21}| + q(p)|,\ q(p) = \ln\left(\frac{r_{21}^p - s}{r_{32}^p - s}\right), s = 1.sgn(\epsilon_{32}/\epsilon_{21}), \emptyset_{ext}^{21} = \left(r_{21}^p \emptyset_1 - \emptyset_2\right)/\left(r_{21}^p - 1\right),$

$e_a^{21} = \left|\frac{\emptyset_1 - \emptyset_2}{\emptyset_1}\right|,\ e_{ext}^{21} = \left|\frac{\emptyset_{ext}^{21} - \emptyset_1}{\emptyset_{ext}^{21}}\right|,\ GCI_{fine}^{21} = \frac{1.25 e_a^{21}}{r_{21}^p - 1}$

The three sets of grid points, i.e., 723, 241, and 121, corresponding to grid sizes 0.01 m, 0.03 m, and 0.06 m, respectively, have been used to calculate the GCI. Where N is the number of grid points; r is the grid refinement factor; p is the apparent order of the method; $\emptyset_{ext}$ represents the extrapolated value; e_a and e_{exit} represent approximate and extrapolated relative error, respectively; and GCI_{fine} is the fine grid convergence index. The numerical uncertainty of the fine grid set (N_1 and N_2) is 0.55%, and for the coarse grid set (N_2 and N_3) is 1.51%. Therefore 241 grid point is selected for further study.

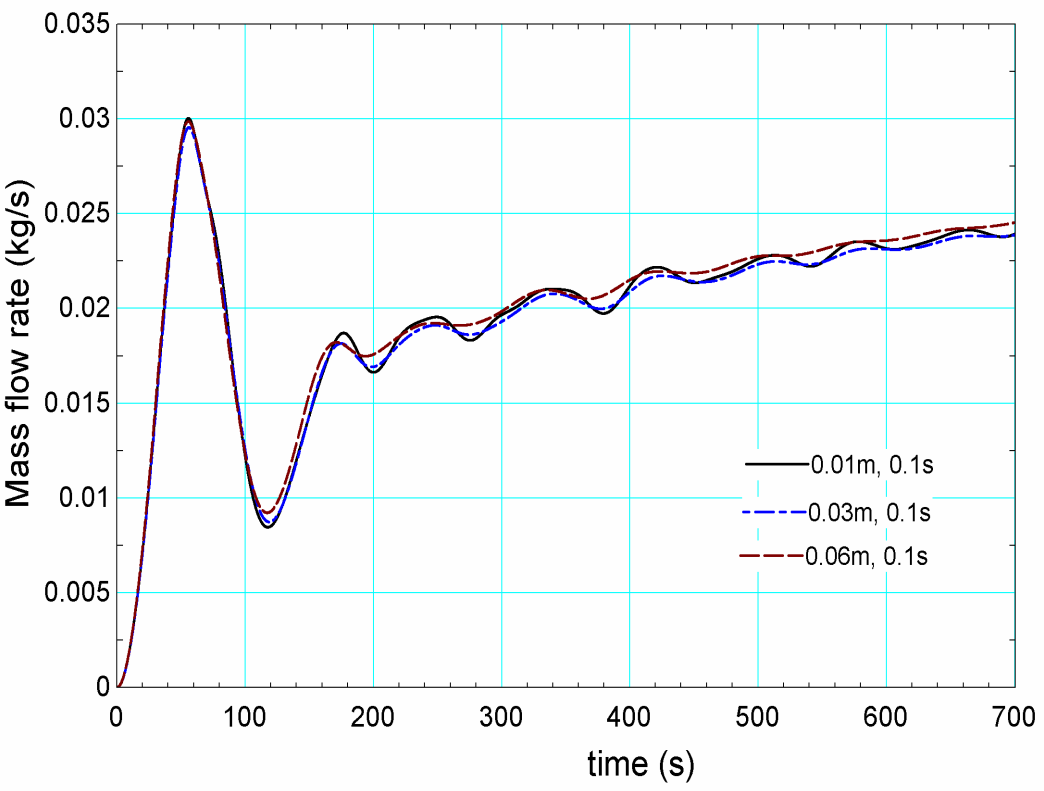

(a)

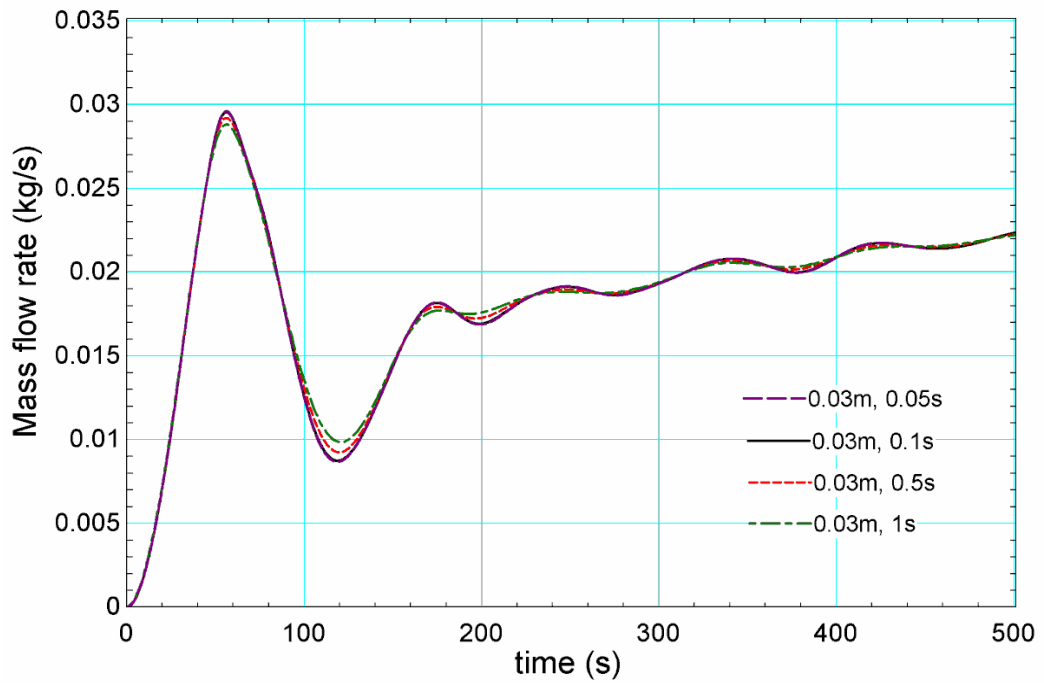

(b)

Fig. 3.3 Temporal variation of mass flow rate for (a) different grid sizes and the time-step Δt = 0.1 s and (b) different time steps and the grid size of 0.03 m.

3.1.6 Model validation

The numerically obtained data for the transient and steady-state simulations have been compared with the measured values by Vijayan et al. [97] for VHHC orientation of SPNCL with water as the primary fluid. The relevant geometrical parameter are loop diameter = 26.9 mm, loop height = 2.2 m, loop width = 1.415 m, and inlet temperature for coolant = 30^{o}C. The predicted and experimental values for the steady-state mass flow rate of water with input heating power of 100 – 1000 W are shown in Fig. 3.4a. The figure reveals that the average deviation between the numerical and experimental values is about 8.1%. Similarly, a comparative assessment between the computed and experimentally obtained time-dependent pressure drop showed a maximum deviation of about 7.3%, which is well within the experimental uncertainty limits and acceptable for a practical purpose (see Fig. 3.4b).

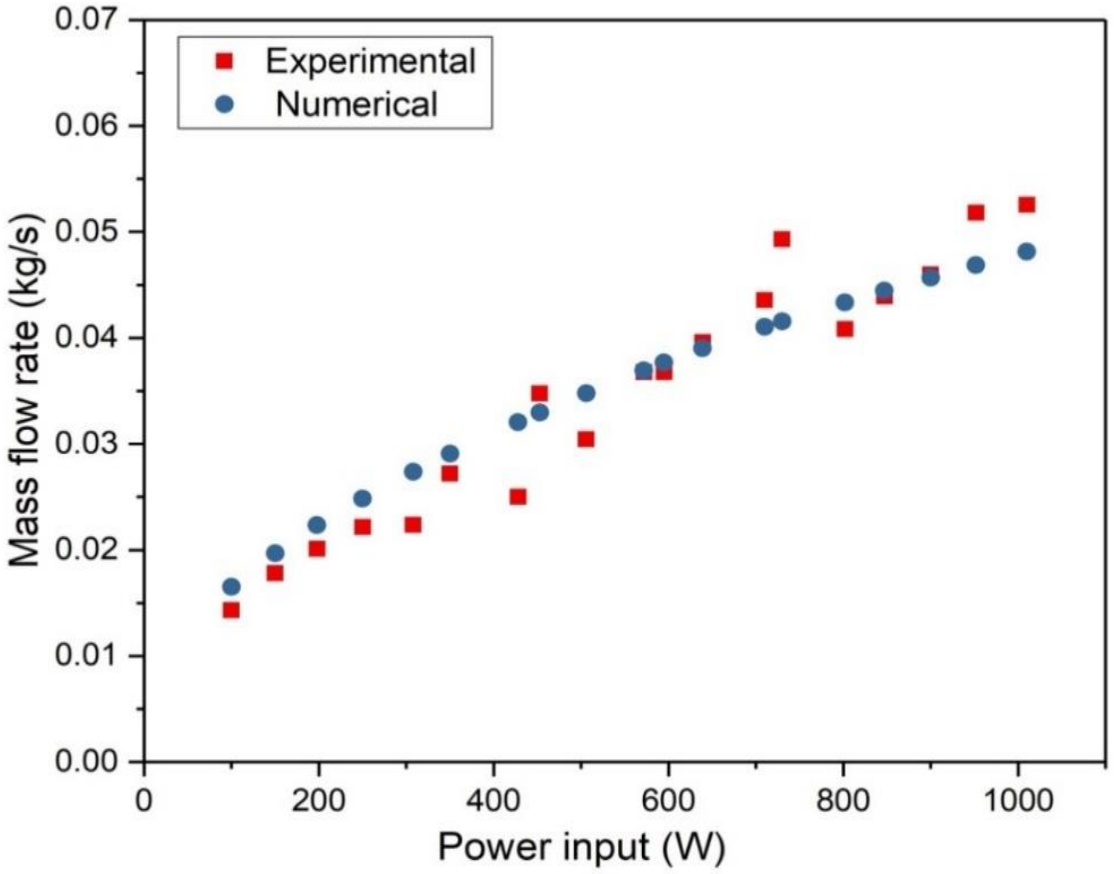

(a)

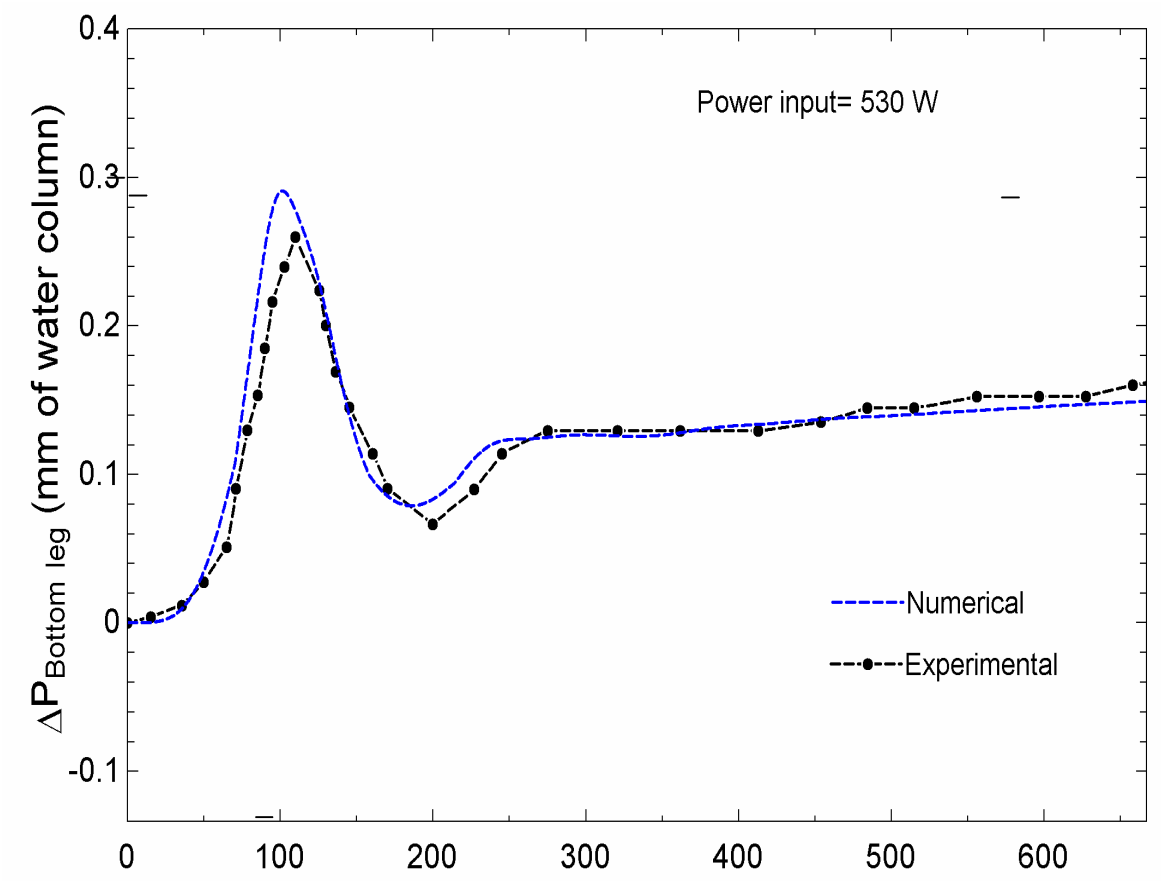

(b)

Fig. 3.4 (a) Comparison of numerical mass flow rate with experimental at the steady-state. (b) Comparison of transient pressure drop with experimental result by Vijayan et al. [97].

3.2 Results and discussion

This section shows the results and discussion on the performance of VHHC configuration of SPNCL using various working fluids.

3.2.1 Water-based binary hybrid nanofluids

The transient and steady-state behaviors of VHHC SPNCL are evaluated for different water-based binary hybrid nanofluids (Al_2O_3+Ag, Al_2O_3+Cu, Al_2O_3+TiO_2, Al_2O_3+CNT, Al_2O_3+Graphene), heater power, tube diameter, loop height, and loop inclination. In the simulation, 1% volume concentration of nanoparticles is considered, which has been

reported as optimum for heat transfer applications [113]. Geometric and operating conditions for the loop are summarized in table 3.4.

Table 3.4 Operating condition and geometric parameter used in this analysis.

Input Parameters	Values/Range	Mean value
Loop diameter (internal)	20, 25, 30 mm	25 mm
Loop Height	1.4, 2.2, 3 m	2.2 m
Loop inclination	0^o, 15^o, 30^o, 45^o	0^o
Loop width	1.415 m	-
Heating length	0.73 m	-
Cooling length	0.80 m	-
Coolant Inlet temperature	301 K	-
Power input	100, 500, 1000 W	500 W
Nanoparticle volume concentration	$\phi = 1\%$	-

3.2.1.1 Flow initiation of SPNCL

The temporal evolution of mass flow rate and Spatio-temporal development of temperature from no flow condition to the steady-state has been shown in Fig.3.5a at a given power of 100W for water. Initially, the loop fluid was in a stagnant condition having a temperature equal to the coolant temperature. As soon as heating is activated, the primary fluid temperature in the heater increases up to 303 K at an instant given by t=25s. At the same instant, a sudden increase of fluid temperature between the heater and the connecting hot leg portion is evident. The fluid temperature in the rest of SPNCL remains unchanged. This is due to an inadequate buoyancy to overcome the friction loss for initiating the flow in SPNCL. As time progresses, for given power input, the generated buoyancy force

eventually exceeds the frictional resistance. This results in the setting up of natural convection in the loop and the hot plug moves upward, and the heater is occupied with cold water. The mass flow rate attains the maximum value at an instant t = 100s (see Fig 3.5b). At this instant, the hot plug shifts towards the horizontally mounted cooler in the top leg of SPNCL and has a maximum temperature difference between the left vertical leg and right vertical leg (see Fig 3.5a), leading to maximum buoyancy force. Afterward, the flow retards up to t = 200 s, and the hot plug enters the cooler. Therefore, the presence of cold fluid in the left leg leads to a minimum temperature difference between the left and right vertical leg, leading to minimum buoyancy force. Subsequently, after t=200s, again hot plug is formed and moves upward, which results in a sudden rise of the mass flow rate and then decreases when the hot plug enters the cooling section. This process continues until the buoyancy force reaches an equilibrium with the frictional force, and at t=2000s steady-state condition has been reached. At the steady-state condition, the cold leg and hot leg temperatures become the inlet temperature for the heater and cooler, respectively.

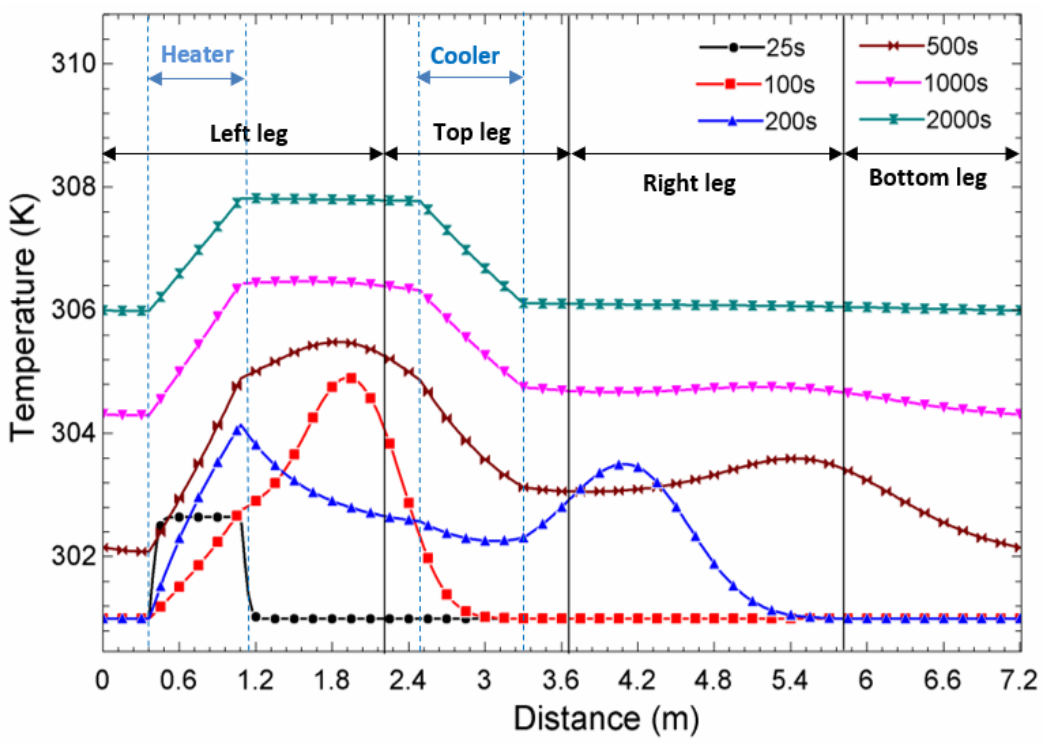

(a)

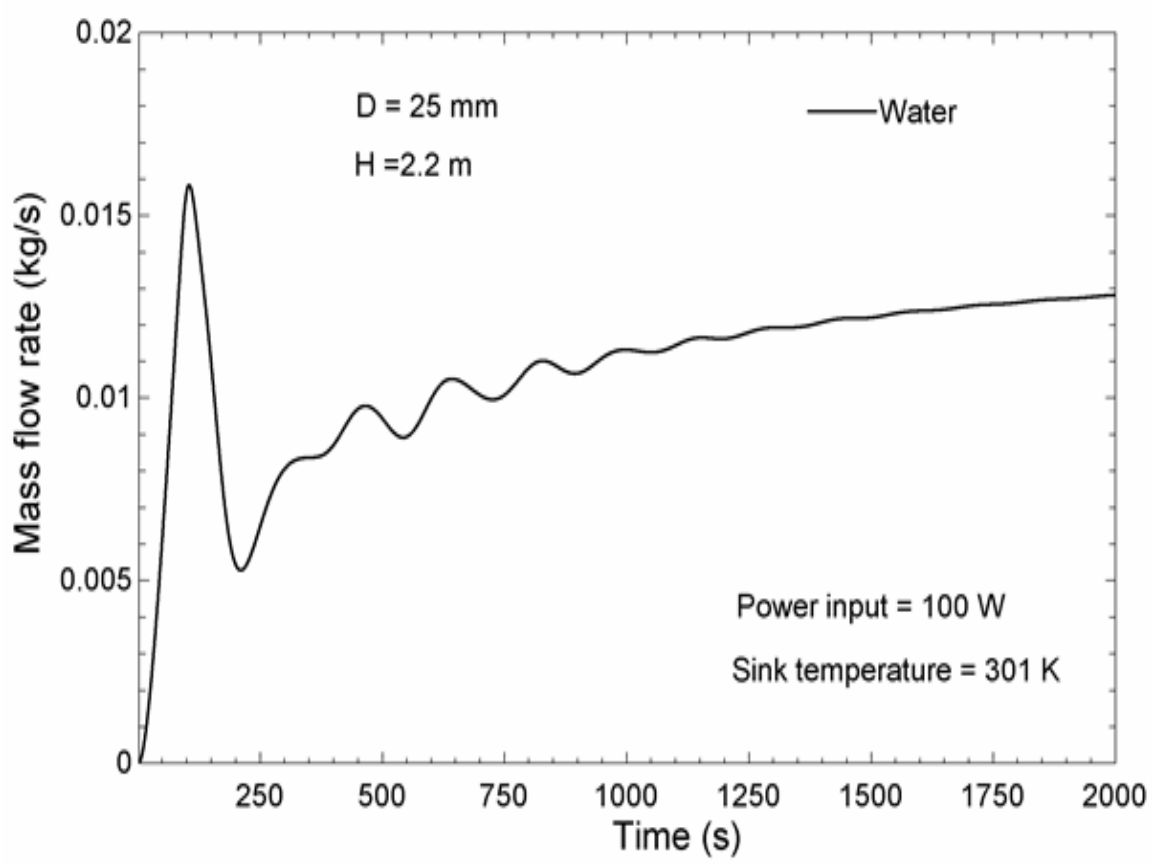

(b)

Fig. 3.5 Variation of primary fluid (a) temperature along the loop at various instants of time (b) Temporal mass flow rate.

3.2.1.2 Transient behavior of SPNCL

The transient variation of mass flow rate in SPNCL with water and binary hybrid nanofluids has been illustrated in Fig. 3.6. This reveals the oscillatory nature of the mass flow rate up to 500 s that eventually stabilizes for both the Water and hybrid nanofluids. The decay in oscillation indicates the setting up of natural convection and that the flow rate attains a particular value as a consequence of the balance between buoyancy and frictional forces. Detailed analysis reveals the development of hot plug in the heater with the initiation of heat input. Subsequently, the established temperature difference between adiabatic hot and cold leg overcomes the frictional force, leading to a sudden increase in the mass flow rate

at about 56s. As the flow rate establishes, the amplitude of oscillations decays to a steady flow condition. The amplitude of oscillation is lower for the hybrid nanofluids compared to water. The relative maximum amplitude of oscillation for water, Al_2O_3+Ag, Al_2O_3+Cu, Al_2O_3+TiO_2, Al_2O_3+CNT, Al_2O_3+Graphene is 70%, 67%, 68%, 68.44%, 68.5% and 68.6%, respectively. These are quite comparable; however, the time required to attain the steady-state reduced from 1002 s for water to 826 s for Al_2O_3+Graphene. This is certainly an advantage considering its application in the cooling of nuclear reactors, which may mitigate the risk of severe accidents to a certain extent. The relative increase in mass flow rate under a steady-state is highest for Al_2O_3+Ag (3%), followed by Al_2O_3+Cu (2.8%), Al_2O_3+TiO_2 (0.5%), While the reduction in mass flow rate is observed for Al_2O_3+CNT (2.4%) and Al_2O_3+Graphene (4.1%) compared to water. This is attributed to the increasing buoyancy force with density, the temperature difference between adiabatic legs (decreasing specific heat), and the thermal expansion coefficient for hybrid nanofluids. On the other hand, the friction loss increases with viscosity and density. Adding nanoparticles to the water, both viscosity and density increase, so the friction force increases. Therefore, the increase or reduction in mass flow rate of hybrid nanofluids compared to water depends on the domination of net change in buoyancy force and friction force. The dominance of the buoyancy force enhances the mass flow rate, while the dominance of the viscous force reduces the mass flow rate. Figure. 3.6 also illustrates the steady-state mass flow rate with hybrid nanofluids having a spherical shape (Al_2O_3+Ag, Al_2O_3+Cu, Al_2O_3+TiO_2) is higher than that of cylindrical (Al_2O_3+CNT) and platelets shape (Al_2O_3+Graphene). These clearly show that the shape and properties of nanoparticle influences the mass flow rate. The lower mass flow rate of hybrid nanofluids having platelets shape (Al_2O_3+Graphene) and cylindrical shape (Al_2O_3+CNT) is due to higher viscosity. A high viscosity may be due to the large surface area to volume ratio of the nanoparticles. More surface area increases the

friction among nanoparticle and fluid particles, increasing the viscosity and, hence, increasing frictional force; as a result, a decrease in mass flow rate. This indicates that the nanoparticle shape has a very significant influence on the performance of Single Phase NCL.

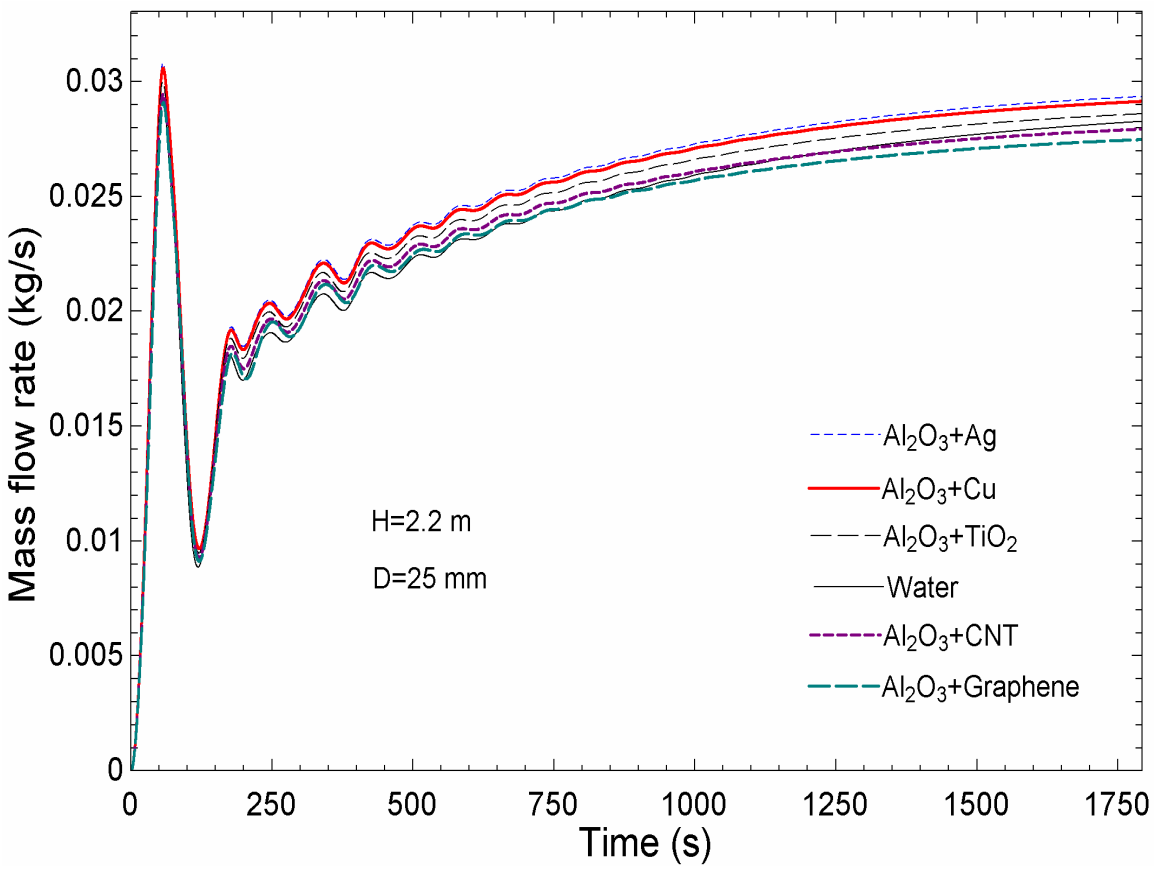

Fig. 3.6 Temporal variation of a mass flow rate of water-based binary hybrid nanofluids at 500 W and 301 K sink temperature.

3.2.1.3 Effect of heat input rate on the transient behavior

The performed simulations are based on the Boussinesq approximation, which is valid for $\beta(T-T_0) \ll 1$. This currently limits the maximum power input up to 1000 W, at which the maximum temperature difference (T_h-T_0) is about 40 ^oC, and the corresponding change in density is less than 2%. The effect of different heater power inputs on the transient mass flow rate has been plotted for the Al_2O_3+Ag+water hybrid nanofluid. Figure 3.7 depicts the early initiation of flow and increasing mass flow rate with heat input, which is attributed to

the resulting buoyancy force due to the elevated temperature difference between adiabatic legs. Obviously, for a high heat input rate, the flow stabilizes at an early instant, which seems to be consistent with Creveling et al. [21].

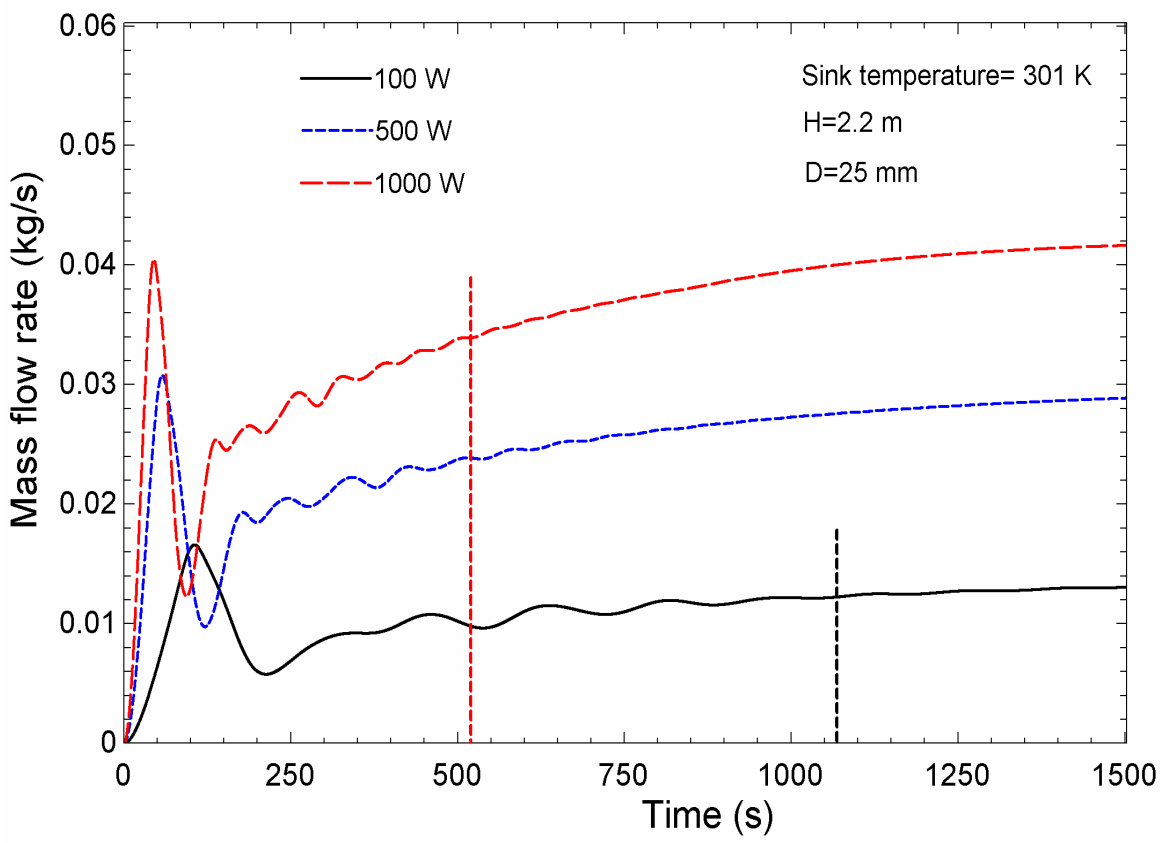

Fig. 3.7 Influence of heater power on temporal mass flow rate for Al_2O_3+Ag hybrid nanofluid.

3.2.1.4 Effect of geometric properties on the transient behavior

In this segment, the influence of the tube diameter and height of the loop on the different performance parameters has been presented. Figure 3.8 demonstrates that the amplitude of fluctuation of mass flow rate and time required to reach the steady-state is least for the smallest diameter of the tube. A possible reason is the increased friction or viscous effect with the decreasing tube diameter at a given power input, which is consistent with the findings of Vijayan et al. [33]. This figure also illustrates that increasing the tube diameter

increases the mass flow rate at a given input power, which is evident from the reduced friction to the fluid flow that varies inversely with tube diameter.

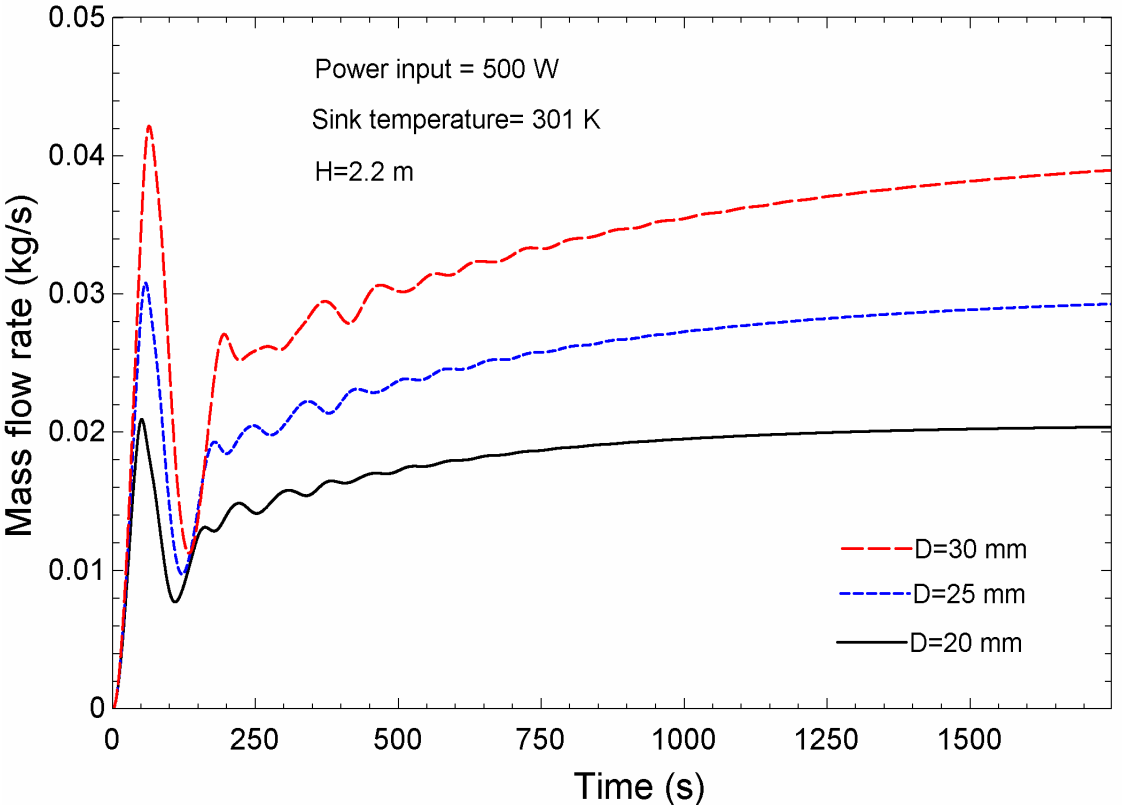

Fig. 3.8 Influence of loop diameter on the temporal variation of mass flow rate for Al_2O_3+Ag hybrid nanofluid.

Figure 3.9 illustrates the influence of loop height on the temporal variation of mass flow rate in SPNCL. It reveals that the highest fluctuations for mass flow rate and longer duration are required to achieve the steady-state for the highest loop height. Furthermore, as a consequence of the buoyancy, the steady-state mass flow rate increases with the height for a specified power input of 500 W. However, the pressure drop also increases due to the loop length corresponding to its height. Thus, the counter effect of buoyancy and pressure drop reduces the relative mass flow rate as the loop height increases.

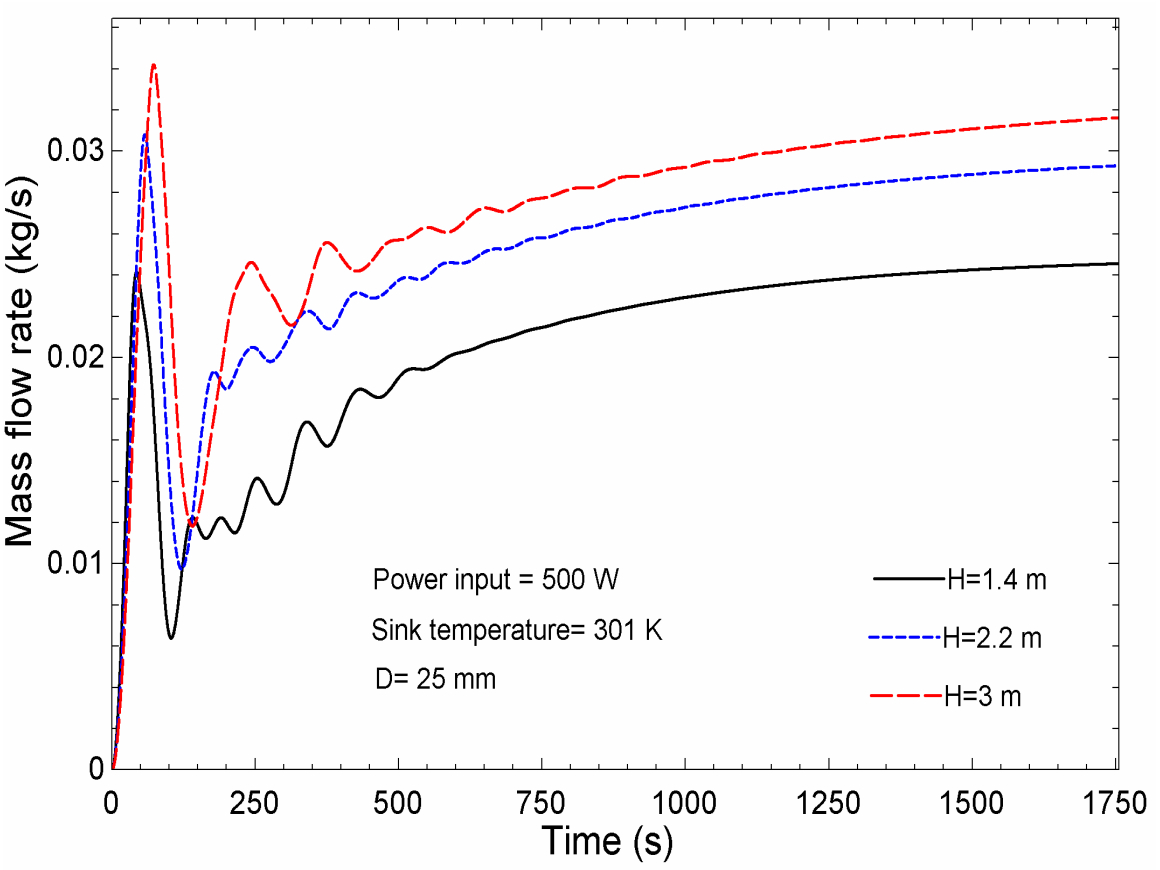

Fig. 3.9 Influence of loop height on the temporal variation of mass flow rate for Al2O3+Ag hybrid nanofluid.

3.2.1.5 Influence of input power on steady-state performance

The steady-state mass flow rates for water-based binary hybrid nanofluids and water at different input powers are illustrated in Fig. 3.10. This shows that the mass flow rate increases with the input power for all the working fluids. This may be attributed to a higher temperature difference between cold and hot legs, which increases the buoyant force relative to the pressure drop. It may be inferred that the spherical-spherical nanoparticle-based binary hybrid nanofluid has a higher mass flow rate than water. Whereas Al_2O_3+CNT+Water and Al_2O_3+graphene+water have a lower mass flow rate up to 500 W (due to their shape), after that, it increases. The possible reason is that at This may be attributed to a higher temperature difference between cold and hot legs, which increases the buoyant force relative to the pressure drop. It may be inferred that the spherical-

spherical nanoparticle-based binary hybrid nanofluid has a higher mass flow rate than water. As the input power increases, the flow regime changes from laminar to turbulent, and therefore, the relative effect of frictional force decreases because of the friction factor, and buoyant force starts dominating because of the suspended nanoparticles. This observation infers that the addition of nanoparticles at a high input power is more beneficial compared to low input power.

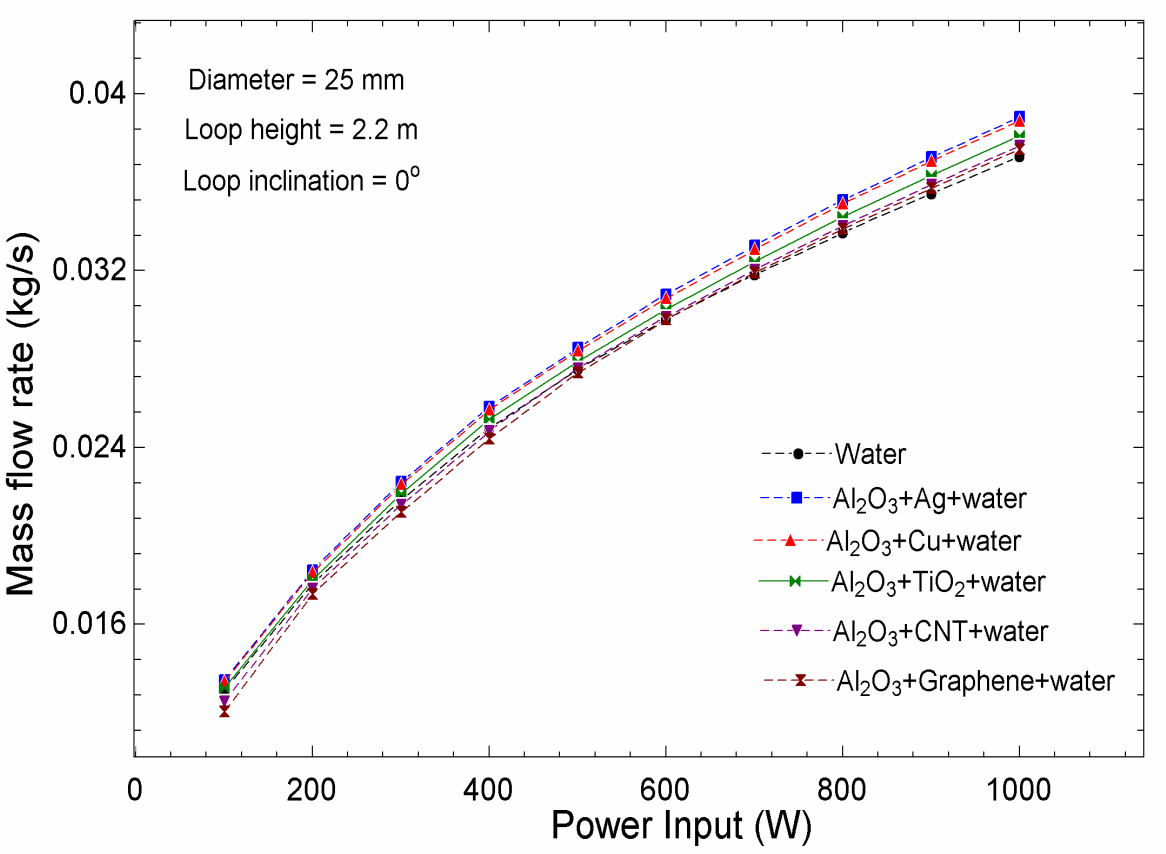

Fig. 3.10 Effect of heater power input on mass flow rate for different binary hybrid nanofluids

The steady-state effectiveness for water and binary hybrid-nanofluids at different input power has been shown in Fig. 3.11. The effectiveness decreases and then increases with the input power. The flow regime changes with the input power; laminar to turbulent flow changes at approximately 400 W (at Re=2300) for water and spherical-spherical shape nanoparticle based binary hybrid nanofluid and approximately 500 W (at Re=2300) for

spherical-Platelets and spherical-cylindrical shaped binary hybrid-nanofluids. In the laminar flow regime, the effectiveness decreases and increases in the turbulent flow regime with the input power. The reason may be that increasing input power increases both the numerator and denominator term in the effectiveness equation (3.25). The increment in the numerator is lower than the denominator for laminar flow regimes due to the lower heat transfer coefficient and higher for the turbulent flow regime due to the higher heat transfer coefficient. Al_2O_3+Graphene shows maximum effectiveness compared to water up to 500 W input power, and Al_2O_3+Ag shows higher effectiveness after 500W.

Figure 3.12 demonstrates the variation of total entropy generation in the loop with respect to heater power input for different binary hybrid nanofluids and water. It depicts that the entropy generation increases with increasing power input. The possible reason is that the entropy generation depends on the irreversibility due to heat transfer and pressure drop. As the power input increases, the heat transfer increases; hence, the entropy generation increases. At a given power, it can be observed that the entropy generation for water is found to be higher than all hybrid nanofluids. This is because at a given power, the entropy generation depends on the temperature ratio (TR) (T_h/T_c), heater wall temperature, and pressure drop. The increase in TR, heater wall temperature and pressure drop increases the entropy generation. The water has a lower mass flow rate and heat transfer coefficient than other hybrid nanofluids. So due to the lower mass flow rate, the temperature difference between the hot leg and cold leg increases; hence, the TR value increases, which results in higher entropy generation. The wall temperature of the heater is also higher due to the lower heat transfer coefficient, which increases the entropy generation. Pressure drop decreases with a decrease in mass flow rate, which reduces the entropy generation. But the magnitude of entropy generation due to pressure drop is negligible; hence it does not provide a

significant effect on entropy generation. Al_2O_3+ Graphene shows a minimum total entropy generation rate compared to water and other binary hybrid nanofluids.

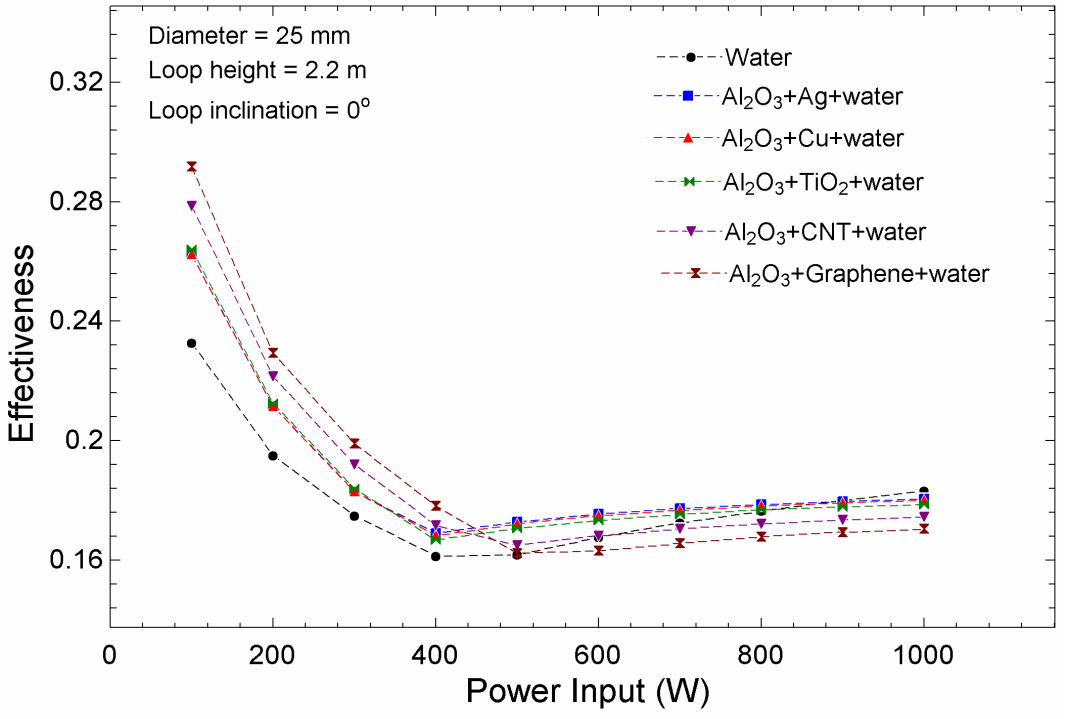

Fig. 3.11 Effect of power input on the effectiveness for different binary hybrid nanofluids

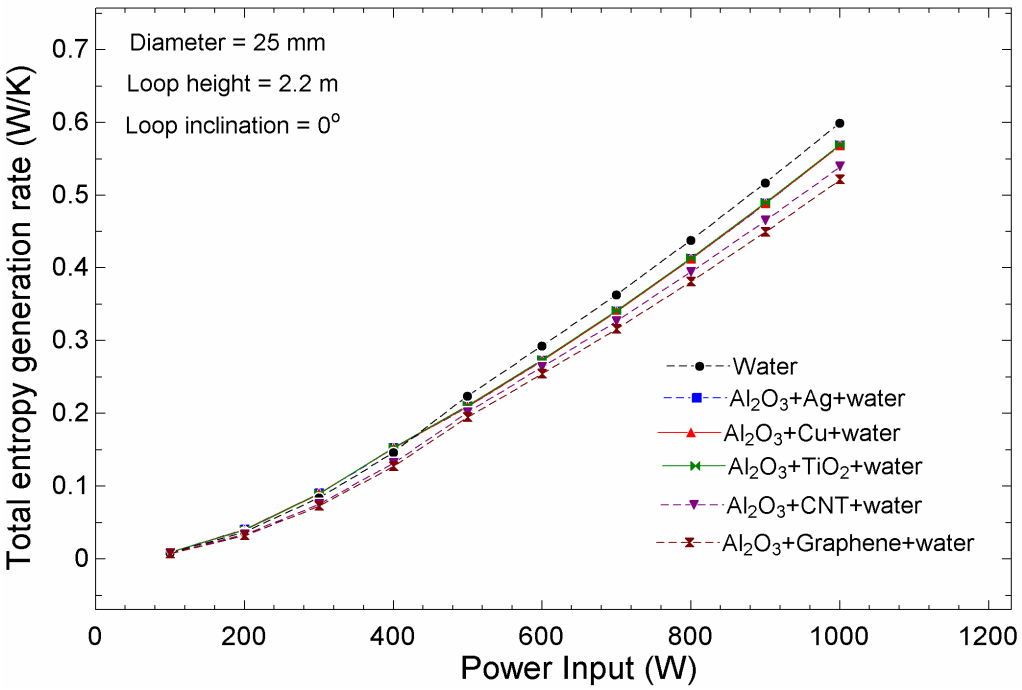

Fig. 3.12 Effect of power input on the total entropy generation for different binary hybrid nanofluids

3.2.1.6 Effect of geometric properties on steady-state performance

The steady-state mass flow rate increases with an increase in tube diameter, as shown in Fig. 3.13. This is because the frictional resistance is inversely proportional to the diameter; hence the friction force decreases with an increase in diameter, and as a result, the steady-state mass flow rate is increased. Figure. 3.14 depicts the effectiveness of the NCL increases with the decrease in the diameter of the loop. The possible reason may be that as the diameter decreases, the mass flow rate decreases, increasing the temperature difference between hot leg and cold leg (T_h-T_c). The heat transfer coefficient is inversely proportional to diameter; hence the heat transfer coefficient increases with a decrease in diameter, and as a result, the temperature difference (T_h-T_0) decrease. Hence, the loop effectiveness increases with a decrease in loop tube diameter. Figure 3.15 represents the effect of loop diameter on the total entropy generation of Al_2O_3+Ag+Water. It can be seen that the entropy generation increases with decreasing diameter of the loop. This is because the mass flow rate decreases with decreasing diameter, which increases the temperature difference between the hot leg and cold leg and TR value, which increases entropy generation. The heater wall temperature also increases, which increases the entropy generation.

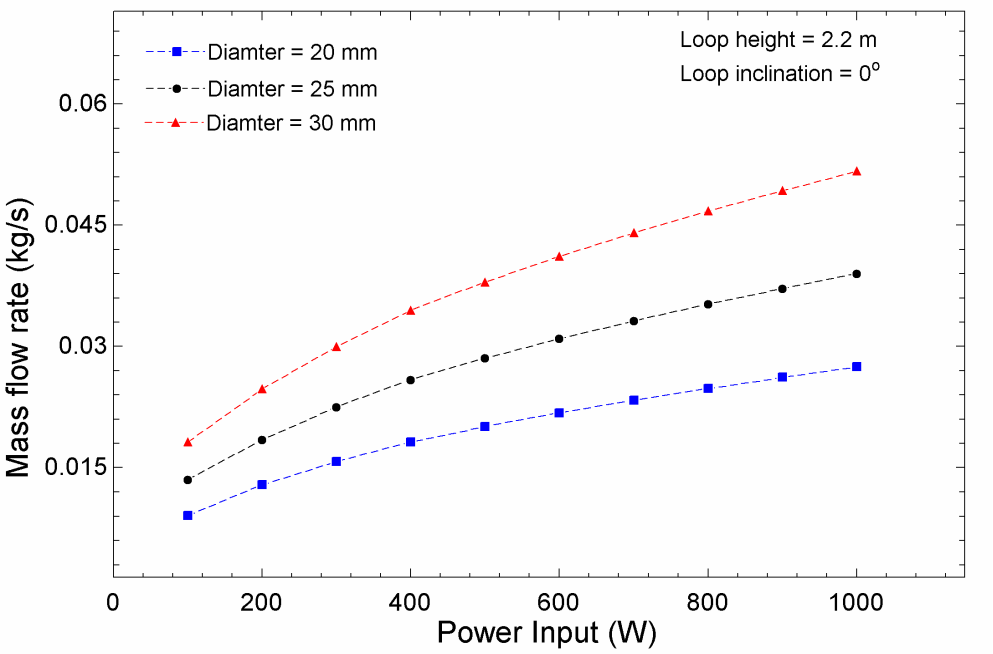

Fig. 3.13 Effect of diameter on steady state mass flow rate for Al2O3+ Ag+ Water hybrid nanofluids

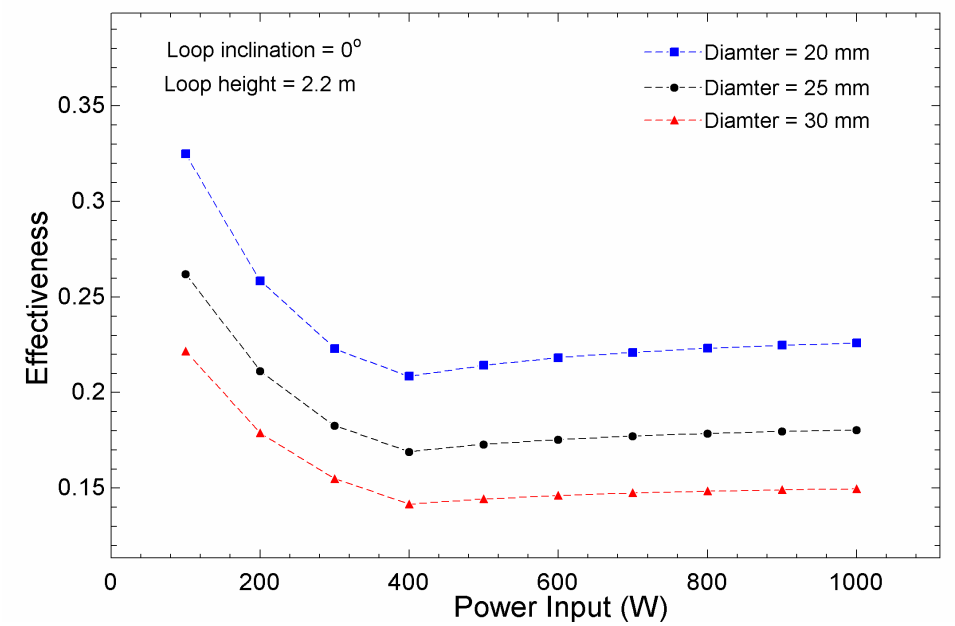

Fig. 3.14 Effect of diameter on the effectiveness for Al_2O_3+ Ag+ Water hybrid nanofluids

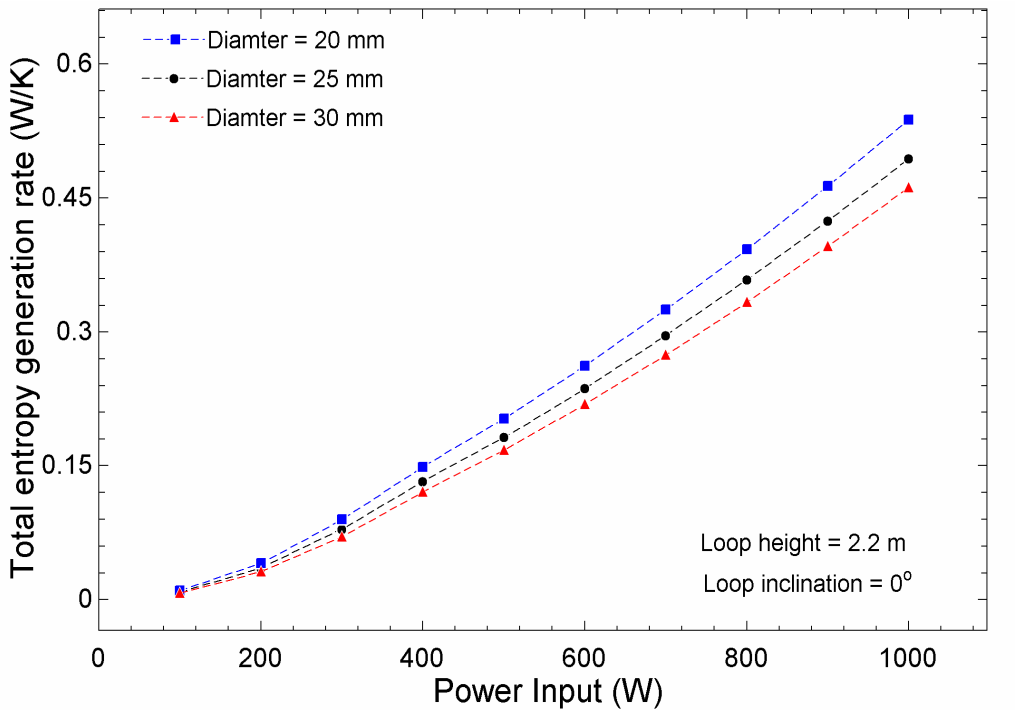

Fig. 3.15 Effect of diameter on the total entropy generation for Al_2O_3+ Ag+ Water hybrid

The buoyancy force increases with an increase in the height of the loop. However, due to the increase in the loop height, the total loop length also increases, increasing the frictional force. Hence increment or decrement in the mass flow rate depends on the dominant one. Figure.3.16 shows that the steady-state mass flow rate increases with increasing height. There is a rapid increment in the mass flow rate from 1.4 m to 2.2 m change in height due to the domination of buoyancy force. But when the height is changed from 2.2 m to 3 m, the mass flow rate increment is reduced due to increased friction resistance. The mass flow rate increases by 20.95% and 8.90% when height is changed from 1.4 m to 2.2 m and 2.2 m to 3 m, respectively at 1000 W. Figure.3.17 depicts the effectiveness decreases with increasing loop height. This is because increasing the height increases the mass flow rate, reducing the temperature difference between the hot leg and cold leg (T_h-T_c). The heat transfer coefficient increases due to an increase in mass flow rate, which reduces the temperature difference (T_h-T_0). Since the numerator and denominator terms are decreasing in the effectiveness equation (3.25), hence the overall effect depends on which has a higher rate of decrement. The numerator has a higher rate of decrement hence the effectiveness is decreasing. Figure 3.18 shows the effect of loop height on the entropy generation of Al_2O_3+ Ag hybrid nanofluid. The increase in loop height increases the mass flow rate, which reduces the temperature difference between the hot leg and cold leg and hence decreases in TR value, which reduces the entropy generation. The heat transfer coefficient increases due to an increase in mass flow rate, which reduces the heater wall temperature; as a result, the entropy generation decreases. The pressure drop increases due to increases in mass flow rate and the total loop length, which increases the entropy generation, but the increment in entropy generation due to pressure drop is very less in the order of 10^{-6}. Hence the total entropy generation decreases with increasing loop height.

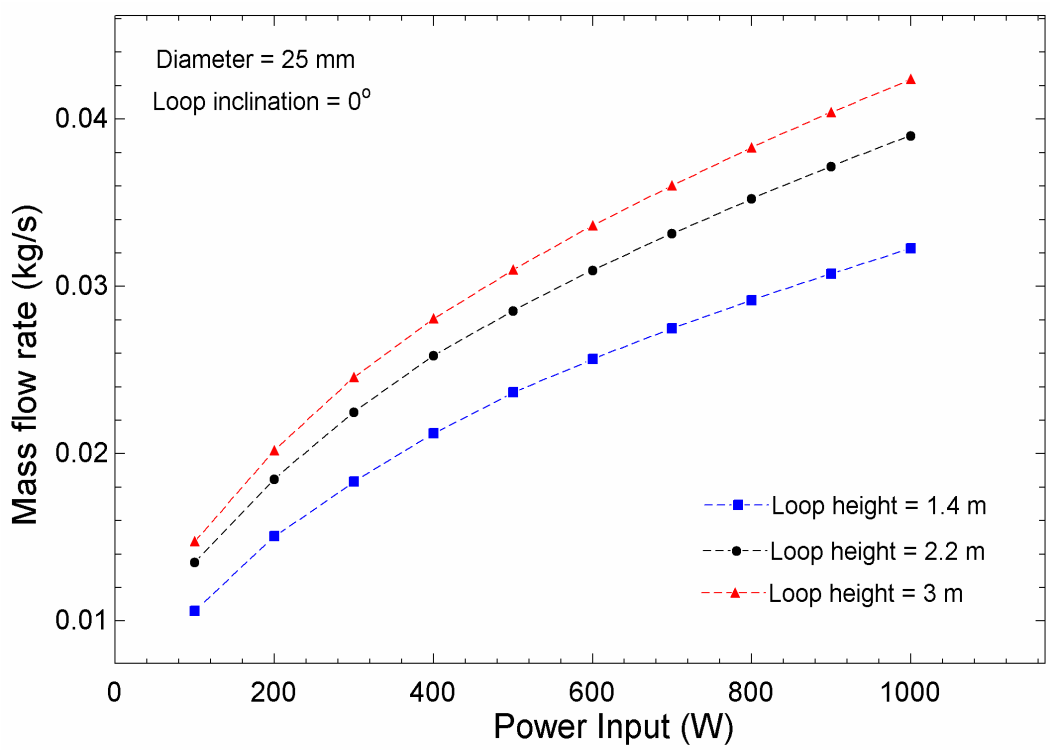

Fig. 3.16 Effect of loop height on steady state mass flow rate for Al_2O_3+ Ag+ Water

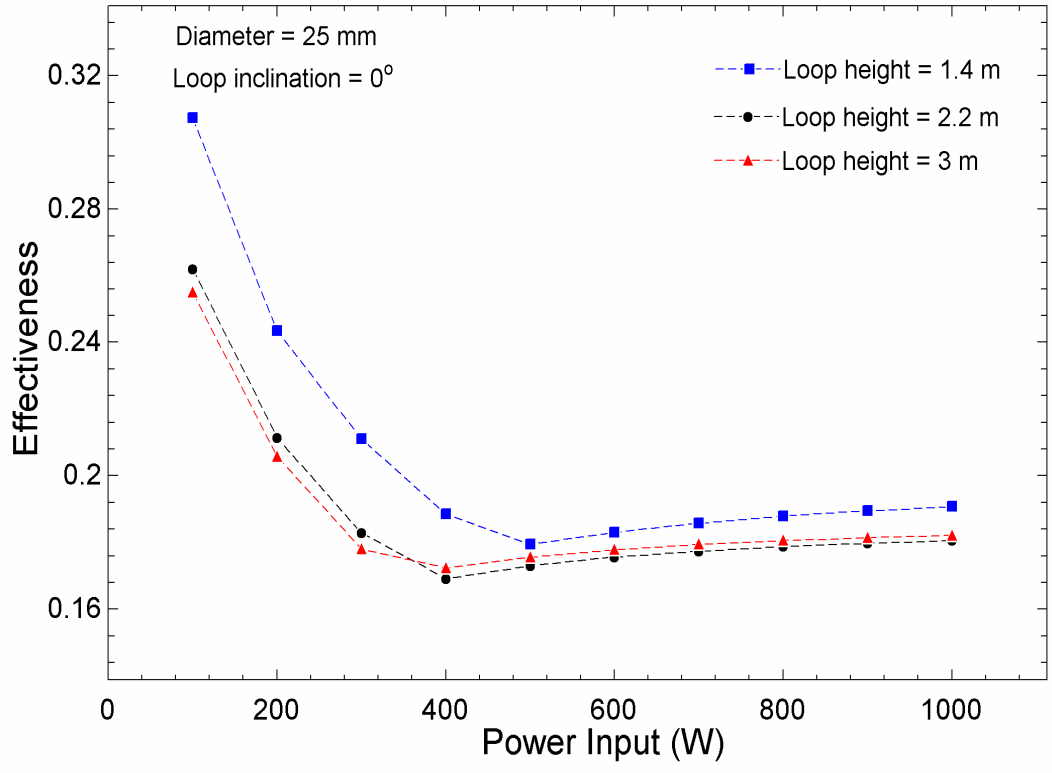

Fig. 3.17 Effect of loop height on the effectiveness for Al_2O_3+ Ag+ Water

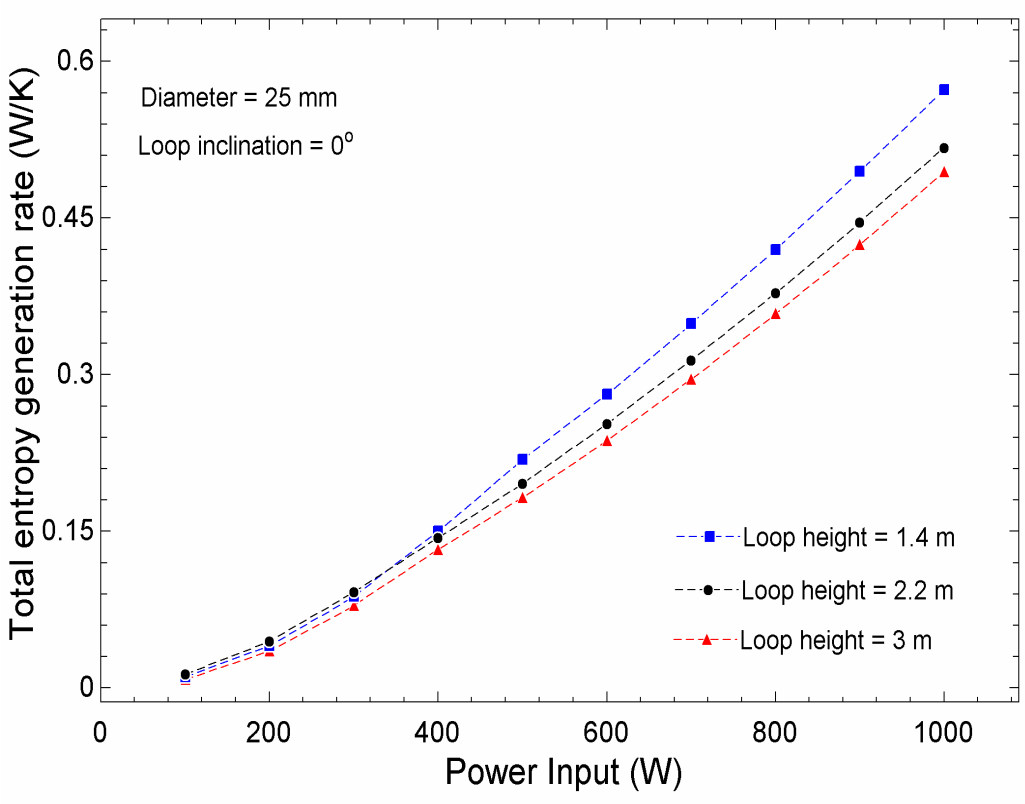

Fig. 3.18 Effect of loop height on the total entropy generation for Al_2O_3+ Ag+ Water

3.2.1.7 Effect of loop inclination on steady-state performance

The inclination of the loop decreases the effective height between the heater and the heat exchanger. As a consequence, the buoyancy force is reduced. However, the total loop length remains unchanged and therefore, the frictional resistance, which leads to the reduction in mass flow rate. Figure 3.19 shows that the reductions for the steady-state mass flow rate at 15^0 and 45^0 loop inclinations are about 14% and 50%, respectively, at an input power of 1000 W. Figure 3.20 reveals the effectiveness of SPNCL increases with the loop inclination. This is attributed to the decreasing mass flow rate with the increasing loop inclination. This leads to an increase in the temperature difference between the hot leg and cold leg (T_h-T_c). The heat transfer coefficient decreases due to a decrease in mass flow rate, which increases the heat exchanger outlet temperature; hence the temperature difference (T_h-T_0) increases. Since both temperature differences, (T_h-T_c) and (T_h-T_0), increase, the

overall effect will depend on which has a higher rate of increment. The rate of increment in the numerator is higher than the denominator; hence the effectiveness is increased. The effect of loop inclination on the entropy generation of Al_2O_3+ Ag+ Water hybrid nanofluid is shown in Fig. 3.21. It is observed that the total entropy generation increases with the increasing loop inclination. The possible reason for that the mass flow rate decreases with increasing loop inclination, which increases the temperature difference between the hot leg and cold leg, hence increasing in TR value which increases the entropy generation. The wall temperature also increases with increasing loop inclination due to a decrease in heat transfer coefficient, which increases the entropy generation.

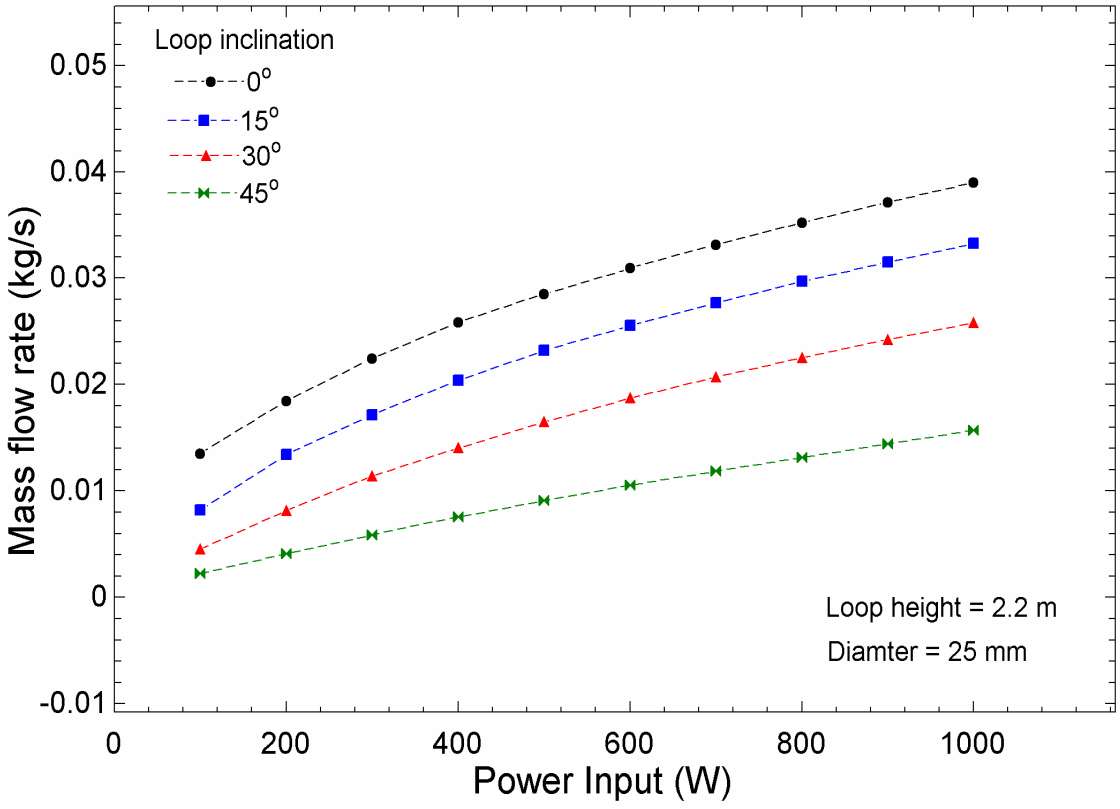

Fig. 3.19 Effect of loop inclination on the steady state mass flow rate for Al_2O_3+ Ag+ Water.

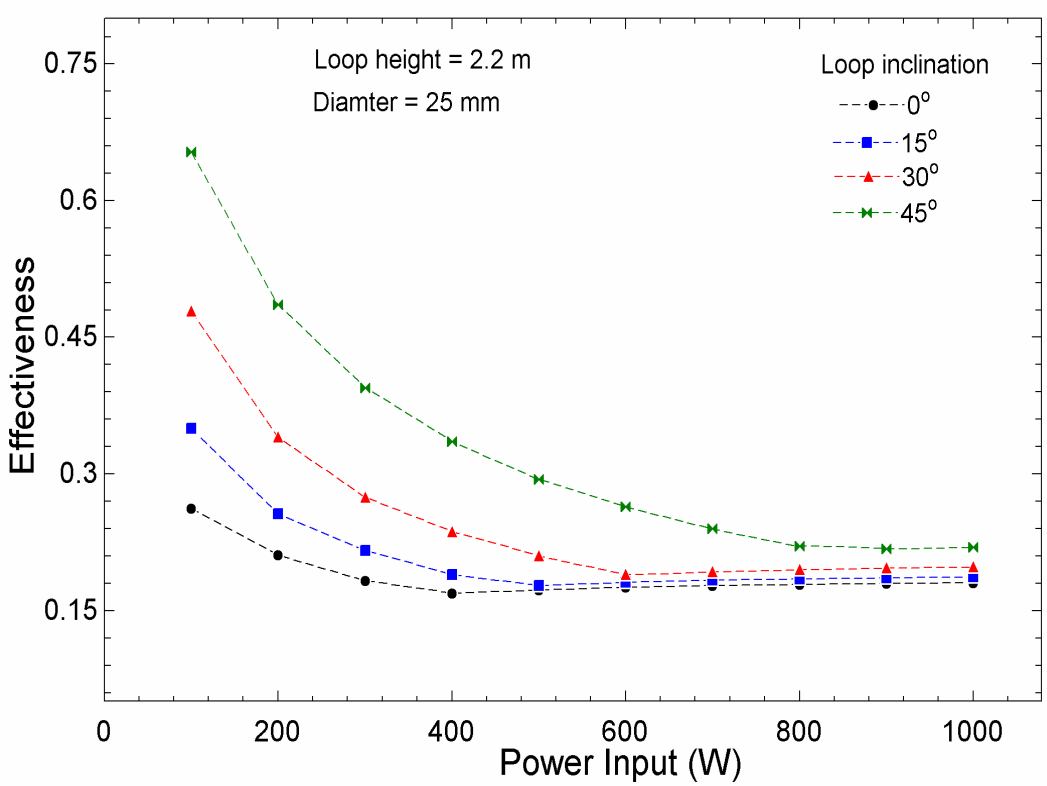

Fig. 3.20 Effect of loop inclination on the effectiveness for Al_2O_3+ Ag+ Water

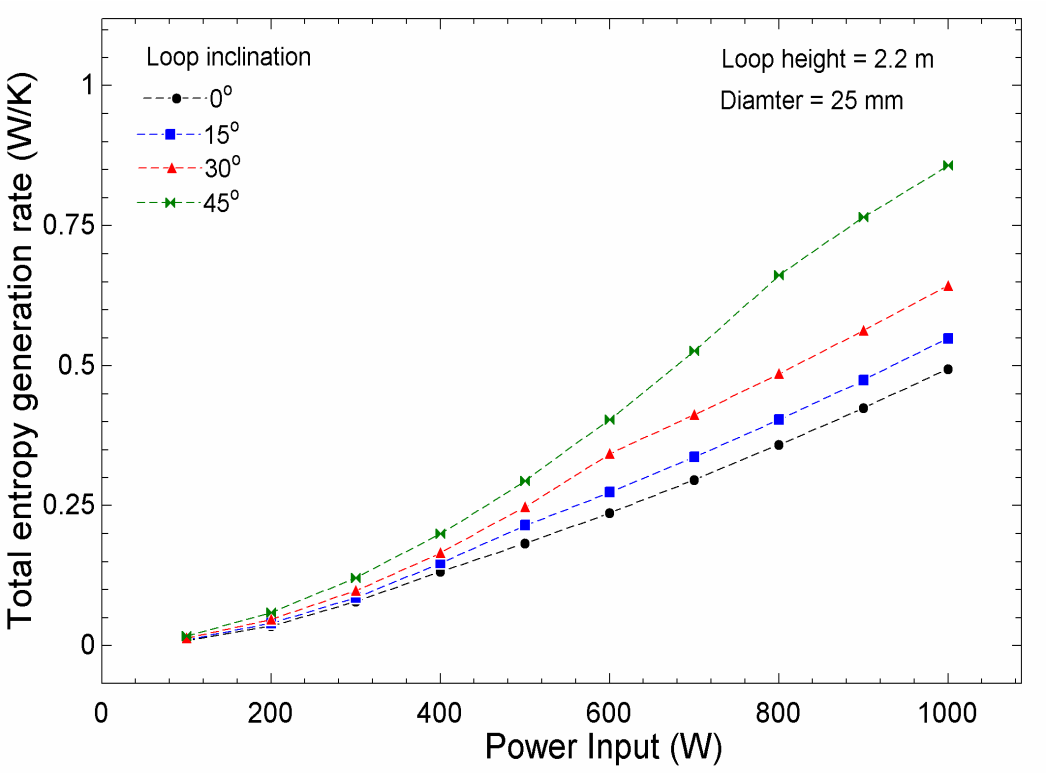

Fig. 3.21 Effect of loop inclination on the total entropy generation rate for Al_2O_3+ Ag+ Water

3.2.2 Water-based ternary hybrid nanofluids

The transient and steady-state characteristics of SPNCL in VHHC arrangement are performed for water-based ternary hybrid-nanofluids, i.e., Al_2O_3+Cu+CNT-water, Al_2O_3+Cu+Graphene-water, Al_2O_3+CNT+Graphene-water, Cu+CNT+Graphene-water. The described performance parameters are computed for the different Input power, loop inclination, and height-to-width ratio. The geometric parameters and operating parameters of SPNCL are summarized in Table 3.5.

Table 3.5 Geometric parameter and operating condition considered in the analysis.

Parameters	Values
Diameter (inner) of the loop	25 mm
Loop Height	2.2 m
Loop width	1.415 m
Length of heating section	0.73 m
Length of cooling section	0.80 m
Loop inclination	0^o-50^o
Inlet temperature of coolant	301 K
Heater input power	100-900 W
Volume concentration	$\phi = 0.9\%$

3.2.2.1 Transient behavior of SPNCL

The transient behavior of fluid mass flow rate in SPNCL for water and water-based ternary hybrid nanofluids is compared for an input power of 500 W. Fig. 3.22 shows the initial oscillations of mass flow rate for all the working fluids, which damped after 600 seconds. These oscillations may be attributed to the imbalance between frictional force and

buoyancy force, which eventually stabilizes. A better explanation can be offered by analyzing the Spatio-temporal temperature development for Water and Al_2O_3+Cu+CNT-water at 500 W in Fig. 3.23. Initially, the working fluid was stationary for a coolant temperature of 301 K. The moment heating is initiated, the fluid temperature rises and the hot plug is formed in the heating section, and the temperature remains the same at other locations, which can be inferred at 25 seconds. Due to this, the temperature difference is developed between the left leg and right leg, establishing the required buoyancy force to overcome the frictional force. Subsequently, the flow is initiated and finally attains the maximum mass flow rate at t = 55 seconds. At this instant, the maximum temperature difference exists between the left leg and right leg, and the hot plug reaches the top of the left leg and enters the horizontal top section. Afterward, the decreasing mass flow rate infers that the entrance of the hot plug in the top horizontal section, and therefore the fluid in the heating section, attain a lower temperature (due to flow). This leads to the decrease in temperature difference between the left and right leg, and therefore the buoyancy force that eventually leads to the reduction of mass flow rate until 125 seconds. At this moment, the hot plug enters the right leg, and the minimum temperature difference is attained between the left and right leg, which results in the least mass flow rate from the initiation of fluid flow. Again, the mass flow rate increases from t = 125 to 180 seconds. This is attributed to the transport of the hot plug in the bottom horizontal leg within this time interval. During this period, the low-temperature fluid emanates the cooler and enters the right leg, and develops a high-temperature difference between the left leg and right leg. Hence, the buoyancy force attains its maximum. This oscillation exists until the flow attains a steady-state, inferring the embellishment of balance between buoyancy and frictional force. For steady-state, the temperature profile of fluid remains constant over the entire loop. Figure 3.23 illustrates that the maximum temperature in the loop is lower for

Al_2O_3+Cu+CNT+water nanofluid than water. Therefore, the ternary hybrid-nanofluids can be used for a higher input power in the single-phase than Water in SPNCL.

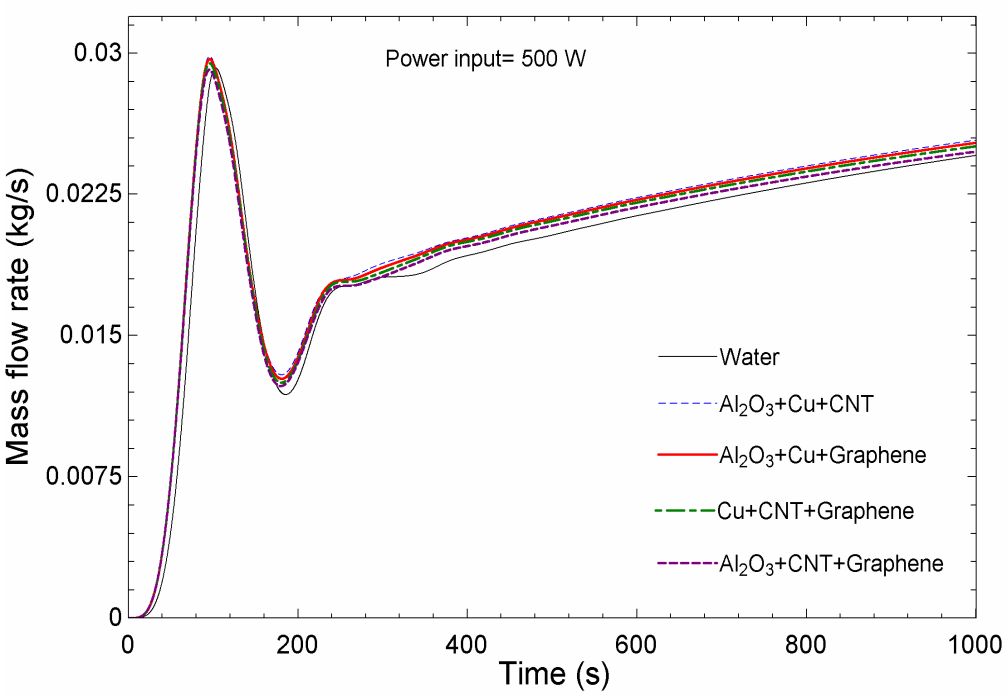

Fig. 3.22Transient variation of mass flow rate for different water based ternary hybrid nanofluids at 500 W input power.

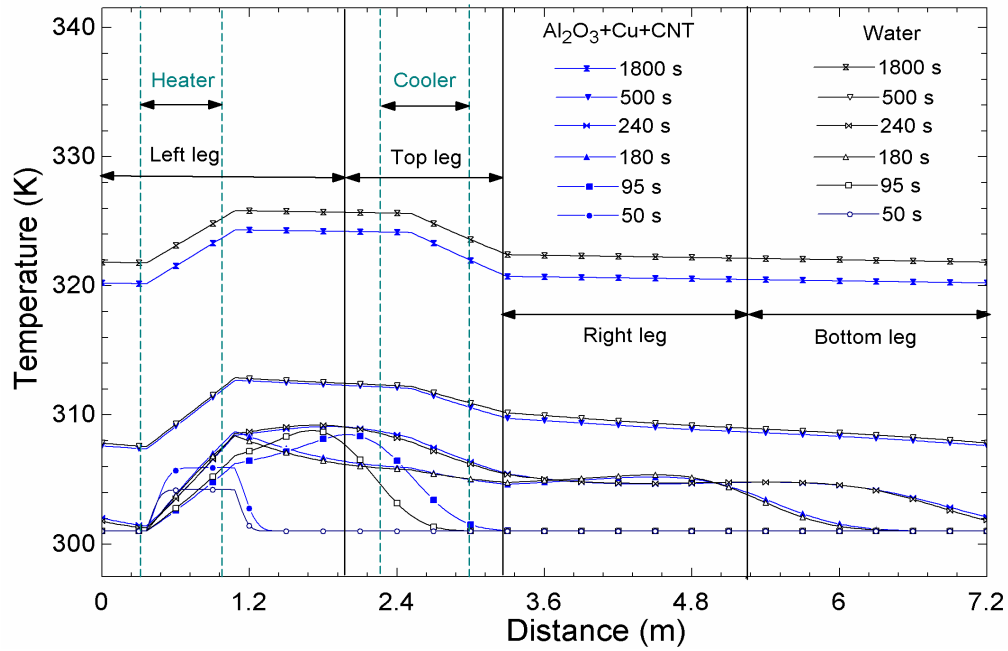

Fig.3.23 The fluid temperature distribution along the loop for water and Al_2O_3+Cu+CNT+water at 500 W power input

The VHHC arrangement for an SPNCL shows the stable flow behavior (without flow reversal) for all the working fluids. But the amplitude of fluctuations and the time required to damp the oscillations are higher for water compared to nanofluids. Therefore, it may be inferred that the use of nanofluids in the SPNCL system allows for achieving the steady-state at an earlier instant of time. The maximum fluctuation in mass flow rate is observed for water (174%) compared to ternary nanofluids (156 to 158.8%). This shows that adding nanoparticles to a base fluid dampens the flow oscillations, which is one of the challenges of SPNCL. Ternary hybrid-nanofluids show a lower steady-state mass flow rate compared to water. This depends on the interplay between buoyancy, promoting the flow, and frictional force, opposing the flow. The buoyancy force is directly proportional to the reference density, volumetric expansion coefficient and hot leg and cold leg temperature difference. The frictional force depends on the density and viscosity of primary fluid. The nanoparticle present in base fluid enhances the buoyancy force due to increases in density and temperature difference (as specific heat decreases); however, the thermal expansion coefficient decreases. The frictional force also increases due to the presence of nanoparticles in the base fluid due to an increase in the viscosity of the nanofluid. The apparent viscosity of nanofluids depends on the shape of the nanoparticles. For instance, a higher ratio of surface area to volume offers higher resistance to the flow on account of the enhanced friction with the fluid particles. The increase or decrease in mass flow rate depends on the relative increase in the magnitude of buoyancy force with respect to the friction force compared to the base fluid. The maximum mass flow rate reduction, in comparison to water, is for Al_2O_3+CNT+Graphene (2.50%), followed by Cu+CNT+Graphene (1.3%), Al_2O_3+Cu+Graphene (0.4%), Al_2O_3+Cu+CNT (0.07%).

Thus, Al2O3+CNT+Graphene (spherical-cylindrical-platelets) attains the lowest mass flow rate among all the ternary hybrid-nanofluids. This is because the platelets shape nanoparticle offers the highest viscosity compared to the other shapes. These show that the nanoparticle shape is a vital parameter for the design of SPNCL.

3.2.2.2 Influence of input power on steady-state performance

The steady-state mass flow rate of ternary hybrid nanofluids and water at different input powers is illustrated in Fig. 3.24. Al_2O_3+CNT+Graphene+water (8.2%) and Al_2O_3+Cu+CNT+water (2.07%) shows the maximum and the minimum decrease in mass flow rate in comparison to water at 100 W input power, respectively. Whereas Al_2O_3+Cu+CNT (0.8%) shows maximum enhancement, and Al_2O_3+CNT+Graphene (1.25%) shows the maximum mass flow rate decrease compared to water at 900 W input power.

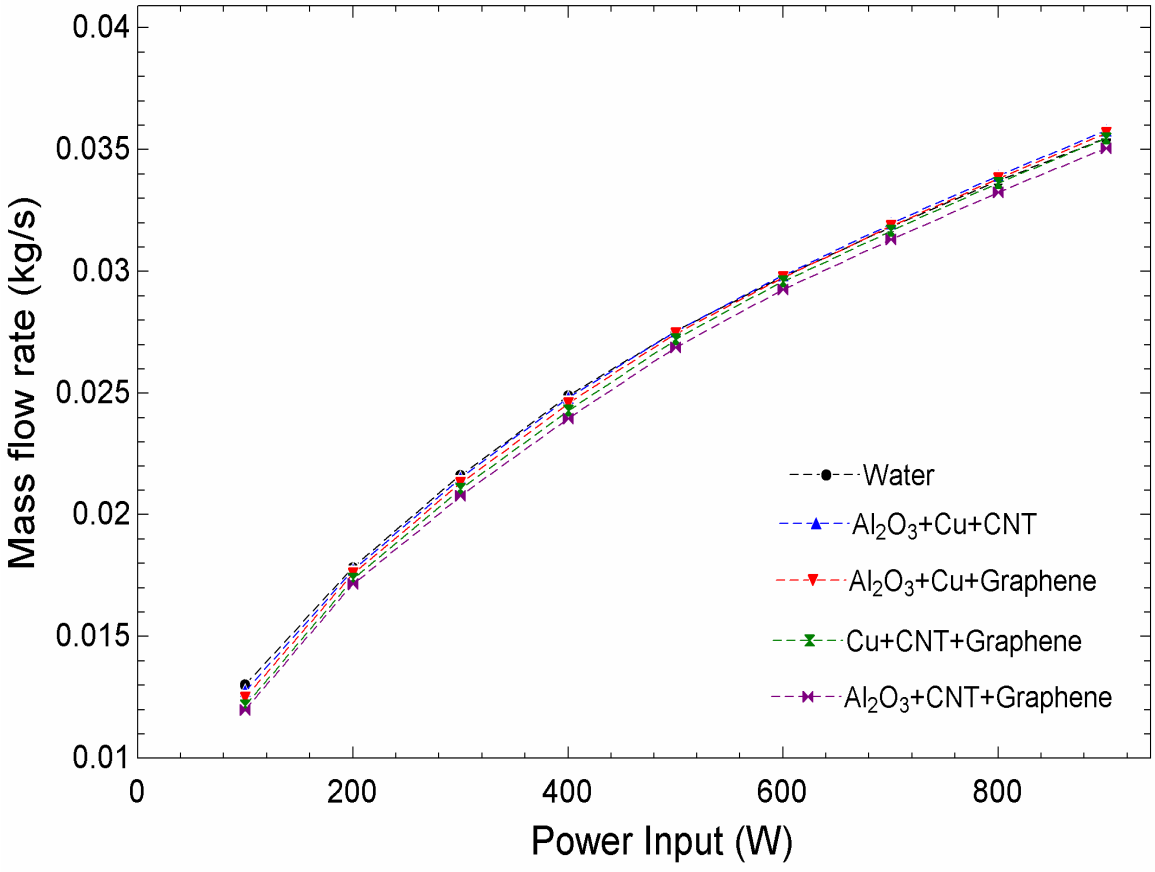

Fig. 3.24 Variation of computed steady-state mass flow rate with input power.

The steady-state effectiveness for water and ternary hybrid-nanofluids at different input power has been shown in Fig. 3.25. The effectiveness decreases and then increases with the input power. Al_2O_3+CNT+Graphene (37.6%) and Al_2O_3+Cu+CNT (29.3%) show maximum and minimum increases in effectiveness compared to water at 100 W input power, respectively. At the highest input power of 900 W, the maximum and minimum enhancement in the effectiveness is for Al_2O_3+Cu+CNT (8.5%) and Al_2O_3+CNT+Graphene (4.5%), respectively.

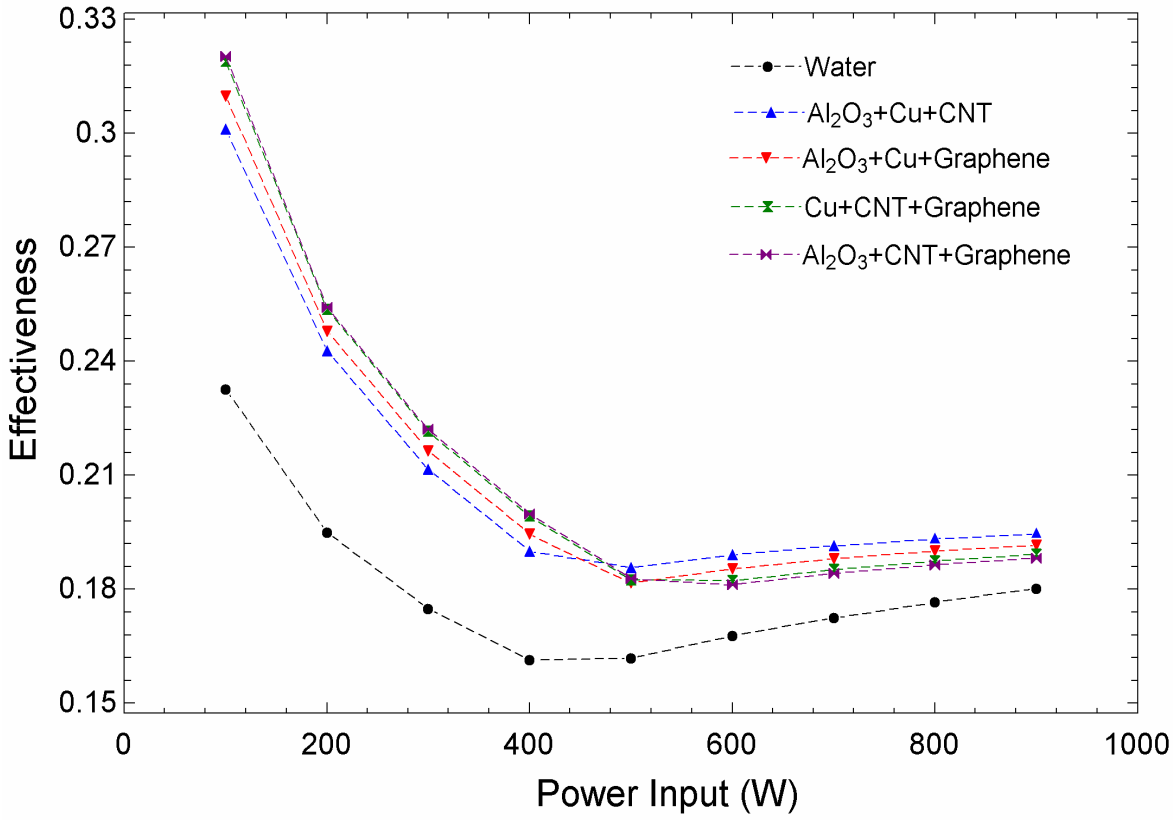

Fig. 3.25 Computed steady-state effectiveness at various input power.

Figure 3.26 shows the effect of input power on the total entropy generation rate for water and ternary hybrid-nanofluids. The figure also shows that the overall entropy generation rate is lower for all the ternary hybrid nanofluids than water, which is desirable in terms of the energetic performance of SPNCL.

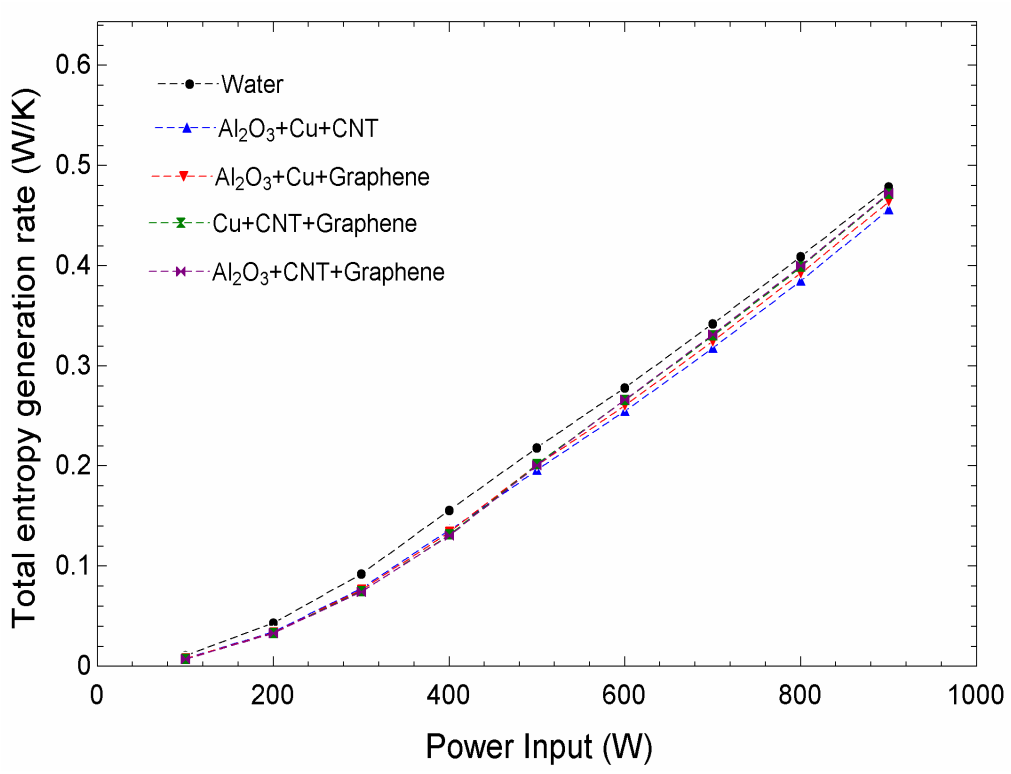

Fig. 3.26 The computed steady-state entropy generation rate various input power.

In particular, Al_2O_3+CNT+Graphene-water shows the maximum reduction in entropy generation rate for an input power up to 450 W, and Al_2O_3+Cu+CNT-water shows the maximum reduction in the entropy generation rate from 450 W to 900 W. Al_2O_3+CNT+Graphene+water (32%) and Al_2O_3+Cu+CNT+water (29%) shows the maximum and the minimum reduction in total entropy generation rate, compared to water, at input power of 100 W, respectively. At the highest input power of 900 W, the maximum and the minimum reduction in the total entropy generation rate is for Al_2O_3+Cu+CNT+water (4.8%) and Al_2O_3+CNT+Graphene+water (1.35%), respectively. The performances of different combinations of water-based binary hybrid nanofluid (Al_2O_3+Cu, Al_2O_3+CNT, Al_2O_3+Graphene, Cu+Graphene and Cu+CNT, CNT+Graphene) and ternary hybrid-nanofluids (Al_2O_3+Cu+CNT+water, Al_2O_3+Cu+Graphene, Al_2O_3+CNT+Graphene, Cu+CNT+Graphene+water) at 100 W power input are shown in Table 3.6. The table shows that the SPNCL system shows better performance with ternary

hybrid nanofluids than binary hybrid nanofluids. Using ternary hybrid nanofluids SPNCL system has a lower reduction in mass flow rate, higher enhancement in effectiveness, and higher reduction in the entropy generation rate than binary hybrid nanofluids.

Table 3.6 The performance enhancement of SPNCL using binary and ternary water-based nanofluid compared to water at 100 W.

Types of hybrid nanofluid	Mass flow rate (kg/s)	Increase (↑)/ Decrease (↓) in mass flow rate (%)	Effectiveness	Increase (↑) in Effectiveness (%)	Total entropy generation rate (W/K)	Decrease (↓) in Total entropy generation rate (%)
Water	0.01303	-	0.2327		0.01073	
Al_2O_3+Cu	0.01336	2.532617 (↑)	0.2621	12.63429(↑)	0.009191	14.343(↓)
Al_2O_3+CNT	0.01256	3.60706(↓)	0.2762	18.6936(↑)	0.008854	17.4837(↓)
Al_2O_3+Graphene	0.01213	6.90714(↓)	0.2883	23.89343(↑)	0.008643	19.4501(↓)

Cu+Graphene	0.01242	4.6815(↓)	0.2864	23.07692(↑)	0.008717	18.7605(↓)
Cu+CNT	0.01285	1.38143(↓)	0.2744	17.92007(↑)	0.00893	16.7754(↓)
CNT+Graphene	0.0117	10.2072(↓)	0.3002	29.00731(↑)	0.008426	21.4725(↓)
Al_2O_3+Cu+CNT	0.01276	2.07214(↓)	0.301	29.3511(↑)	0.007617	29.0121(↓)
Al_2O_3+Cu+Graphene	0.01247	4.29777(↓)	0.3098	33.13279(↑)	0.007487	30.2237(↓)
Al_2O_3+CNT+Graphene	0.01197	8.13507(↓)	0.3202	37.60206(↑)	0.007289	32.069(↓)
Cu+CNT+Graphene	0.01215	6.75365(↓)	0.3189	37.0434(↑)	0.007333	31.6589(↓)

3.2.2.3 Influence of inclination of loop

Figure 3.27 shows the influence of loop inclination on the mass flow rate for different considered ternary hybrid nanofluids and water at 500 W input power. This infers that (a) the mass flow rate reduces with the loop inclination for all the working fluids. With the increasing loop inclination angle φ, the effective height between the heater and cooler decreases, which decreases the buoyancy force, and hence the mass flow rate. The rate of decrease in mass flow rate is more for a higher loop inclination. The mass flow rate decreased by 12.3%, 27.2%, 43.4%, 60.4% and 77.2% at 10^{o}, 20^{o}, 30^{o}, 40^{o} and 50^{o} of loop inclination. Increasing the loop inclination beyond 50° results in the maximum temperature > 373 K in the loop due to a very less mass flow rate. This is undesirable for water-based SPNCL at atmospheric pressure.

Figure 3.28 reveals the effect of loop inclination on the effectiveness of different water-based ternary hybrid-nanofluids and water at 500 W input power. The effectiveness upsurges with the inclination of the loop for all the working fluids. It is due to the fact that the mass flow rate decreases with the loop inclination for all studied fluids. This allows sufficient residence time for primary fluid in the heat exchanger, providing better cooling and hence effectiveness.

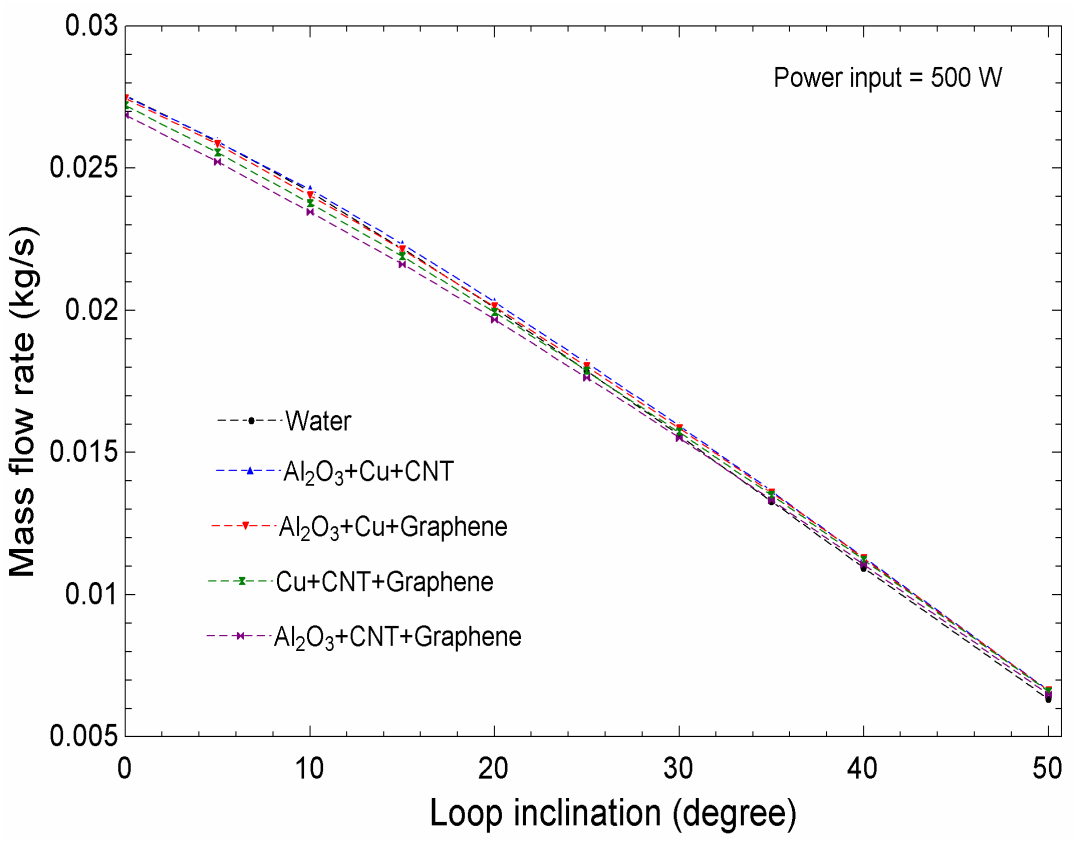

Fig. 3.27 The computed steady-state mass flow rate at various inclinations of loop.

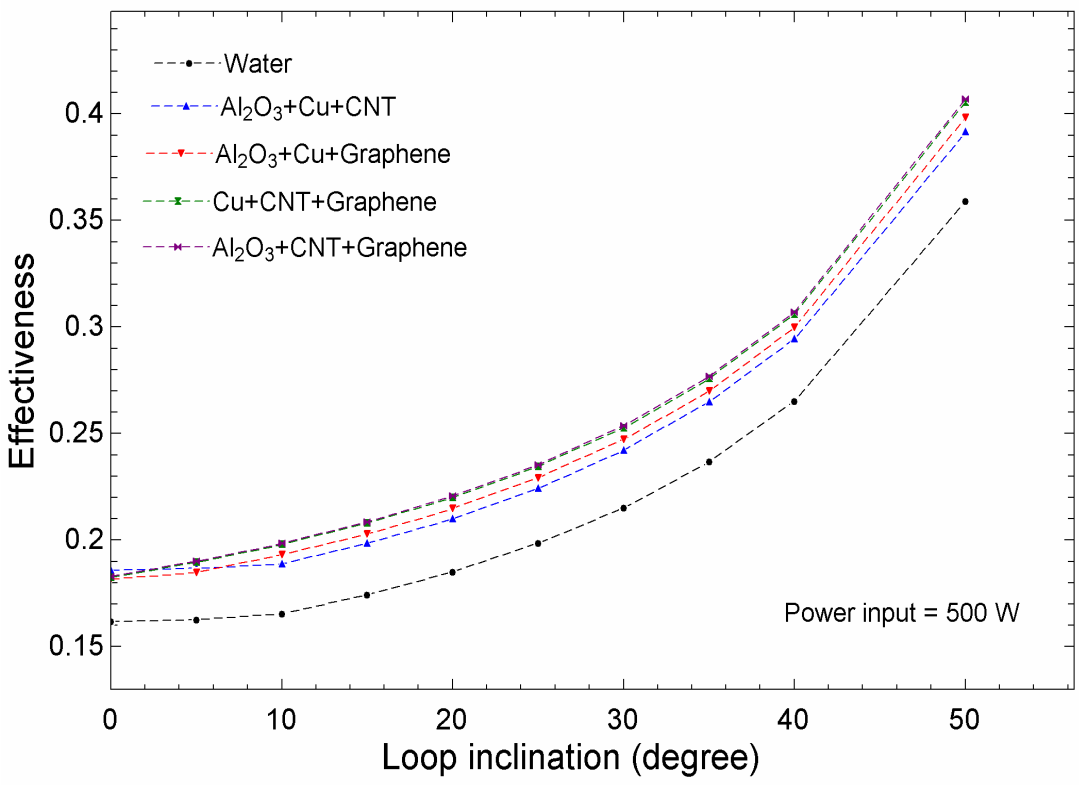

Fig. 3.28 The computed steady-state effectiveness at a various loop inclination angle

Figure 3.29 depicts the influence of loop inclination on the total entropy generation for water and ternary hybrid-nanofluids at 500 W input power. This infers that the entropy generation increases with the increase in loop inclination for given input power. It is because of the reduction in the mass flow rate of fluid, and therefore the temperature difference between hot and cold legs increases, which increases the TR value. As a consequence, the heater wall temperature increases. These combined effects of TR value and wall temperature of the heater enhance the total entropy generation rate. However, the entropy generation rate due to pressure drop decreases, which is negligible compared to the effect of heat transfer.

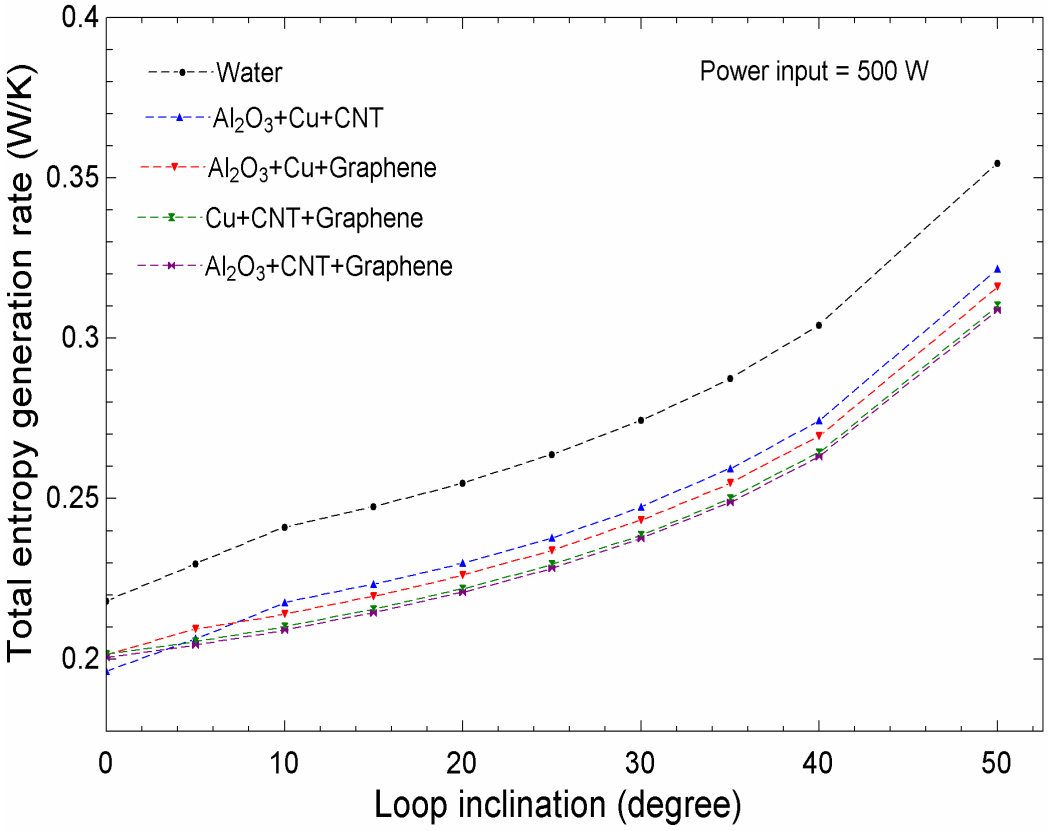

Fig. 3.29 The computed steady-state total entropy generation rate at various loop inclination angle.

3.2.3 Thermal oils

Transient and steady-state characteristics of SPNCL using different thermal oils such as Therminol VP1, Paratherm CR, Dowtherm A and Dowtherm Q have been analyzed and compared with water. The influence of the loop aspect ratio, i.e., height to width ratio, on the performance parameter has also been investigated. The geometric and operating parameter used in this analysis is shown in table3.7.

Table 3.7 Geometric parameter and operating condition considered in this analysis.

Parameters	Values
Diameter (inner) of the loop	25mm
Thickness of the tube	1 mm
Cooler outer tube diameter (internal)	49.2 mm
Loop width	1.415m
Length of heating section	0.73m
Length of cooling section	0.80m
Height -width ratio	0.8-15
Inlet temperature of coolant	301 K
Heater input power	500 W
Total nanoparticle volume fraction	$\phi = 1\%$

3.2.3.1 Transient performance characteristics of thermal oils

The temporal variation of the mass flow rate for different thermal oils and water at a 500 W power input is illustrated in Fig. 3.30. This shows that the flow initiation is earlier and the time required to damp the oscillation is higher for the thermal oils compared to water. The reason is that the thermal oils have a lower viscosity than water at given power input,

hence offering lower frictional resistance. Moreover, the buoyancy force is also higher for thermal oil due to the higher temperature difference between hot and cold legs. The paratherm CR shows the earlier flow initiation and Dowtherm Q shows the higher time to initiate the flow among all the thermal oils.

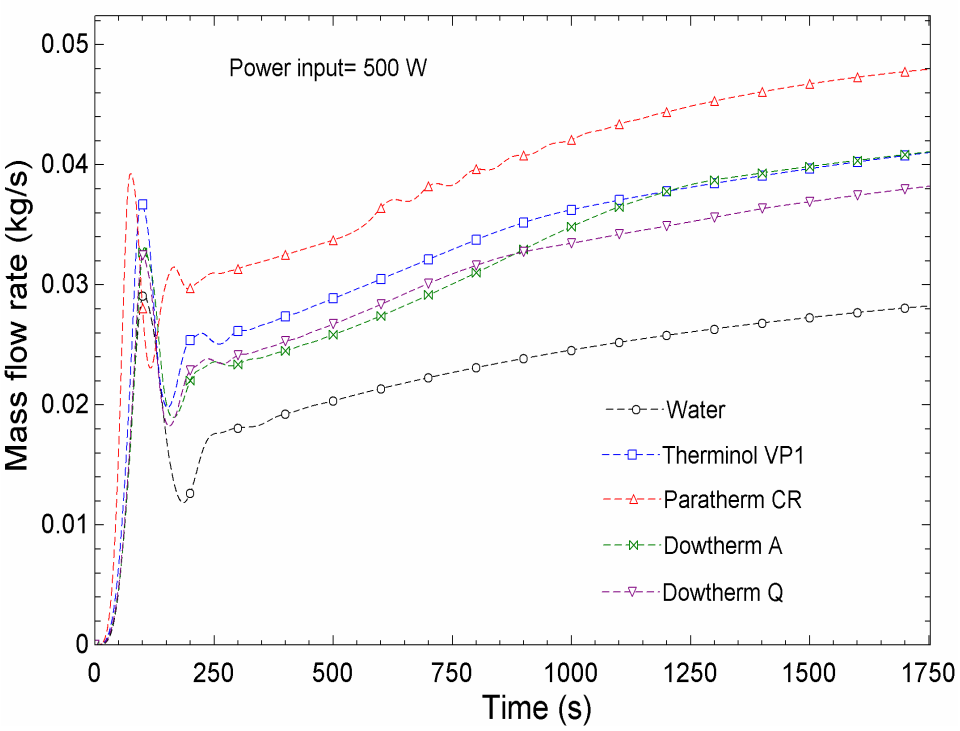

Fig. 3.30 Comparison of transient variation of mass flow rate with water and thermal oils

3.2.3.2 Steady-state performance characteristics

Figure 3.31 illustrates that the mass flow rate for the thermal oils is higher compared to water at 500 W power input. This is because at the same given power input, the change in the temperature difference between hot leg and cold leg is higher (because of lower specific heat) for thermal oil compared to water, which increases the density difference, resulting in higher buoyancy force. The Paratherm CR (70%) shows the highest and Dowtherm Q (50%) shows the lowest increment in mass flow rate compared to water. This reveals that thermal oils can be used as a potential working fluid, which can enhance the heat transport capability of the SPNCL system.

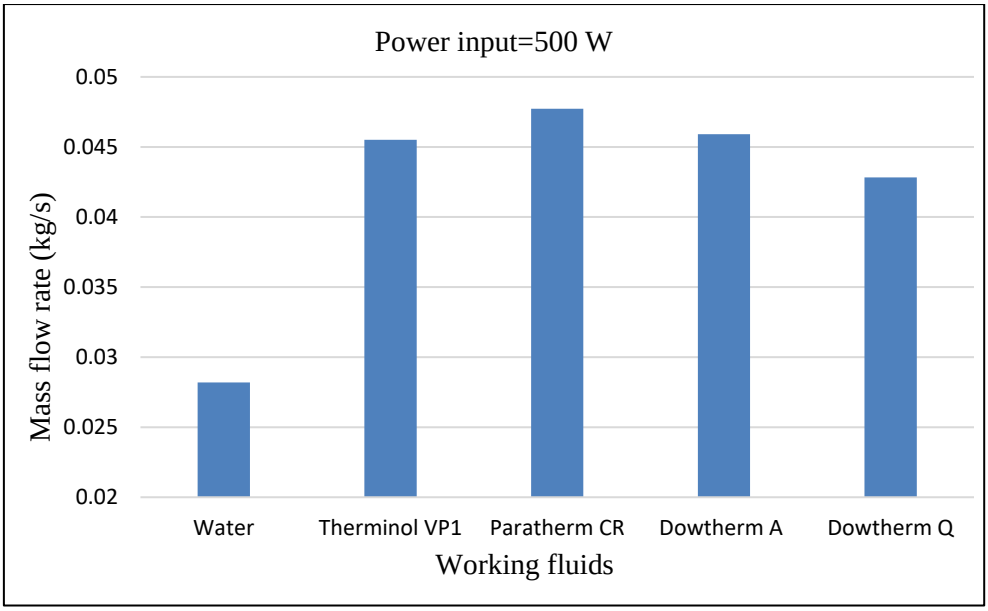

Fig. 3.31 Steady-state mass flow rate for water and thermal oils.

Figure. 3.32 demonstrates the steady-state effectiveness for water and different thermal oils at 500 W power input. It can be seen that the effectiveness for water is higher compared to thermal oils. It may be due to water having higher thermal conductivity compared to thermal oils. Paratherm CR shows the highest and Dowtherm A shows the lowest effectiveness among the thermal oils.

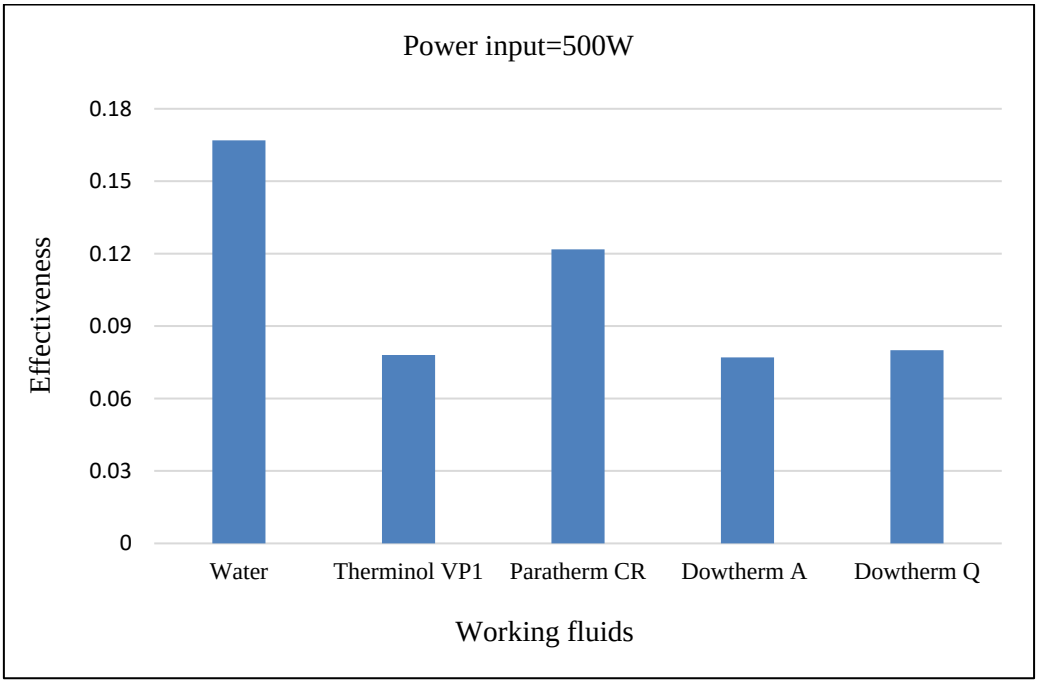

Fig. 3.32 Effectiveness of heat exchanger for water and thermal oils

Figure 3.33 shows that the total entropy generation rate is higher for the thermal oils compared to water. This is because, at the same power input, the temperature difference (T_h-T_c) increases for thermal oil, increasing the TR value, which enhances the entropy generation rate. Also, the heat transfer coefficient for the thermal oils is lower, so the wall temperature increases, which increases the entropy generation; moreover, the pressure drop also increases due to increased mass flow rate, but the contribution of pressure drop is negligible. Hence the total entropy generation for the thermal oil increases compared to water. Paratherm CR shows the best result among all the thermal oils because it has maximum mass flow rate and effectiveness and minimum total entropy generation rate.

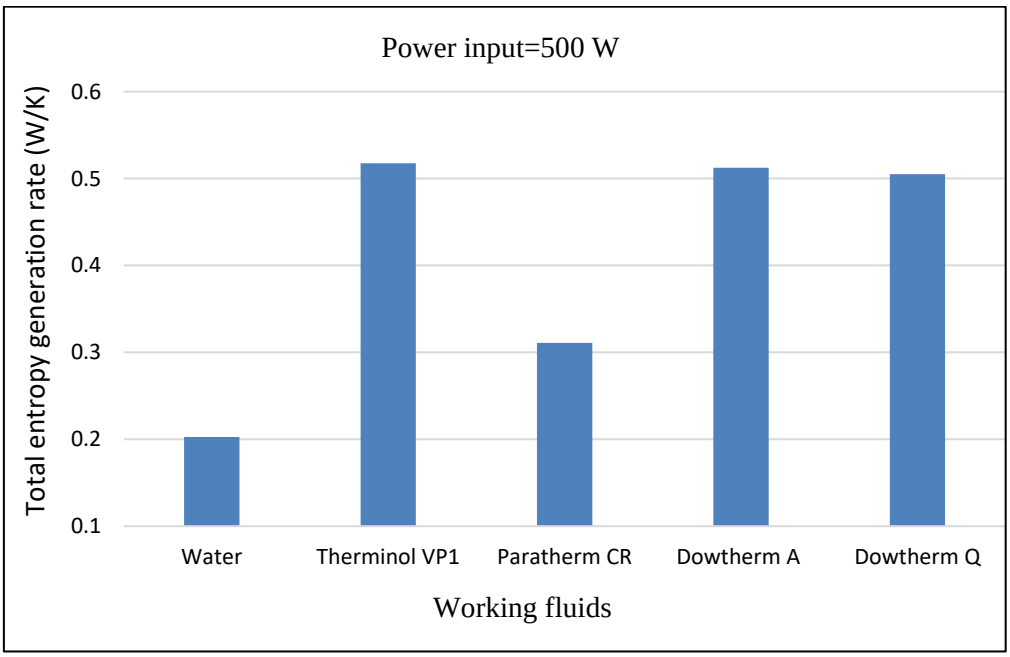

Fig. 3.33 Total entropy generation rate for water and thermal oils

3.2.3.3 Influence of loop aspect ratio (height to width) on performance

The influence of $(H/W)_{ratio}$ on the steady-state mass flow rate, effectiveness, and total entropy generation rate for water and thermal oils is demonstrated in this section. The $(H/W)_{ratio}$ is varied for a fixed width of the loop. Figure 3.34 illustrates the effect of $(H/W)_{ratio}$ on the mass flow rate at steady-state for water and thermal oils. From the figure, it can be observed that the mass flow rate increases with the increasing height-to-width

ratio for water as well as thermal oils. There is a rapid increase in mass flow rate up to $(H/W)_{ratio} = 3$. Afterward, the mass flow rate increment decreases and the rate of increase attains a limiting value for $(H/W)_{ratio} = 14$. These observations can be explained as follows: (a) the increasing value of $(H/W)_{ratio}$ increases the height of the loop or the resulting buoyant force, (b) the increasing $(H/W)_{ratio}$ also increases the length of SPNCL and the resulting friction force. So, the increase in mass flow rate with $(H/W)_{ratio}$ depends on the net increment in the buoyancy force and frictional force. It can be also observed that the increment in mass flow rate is higher for thermal oils as compared to water for the same increase in height to width ratio. An increase in $(H/W)_{ratio}$ from 0.8 to 3 increases the mass flow rate by about 78% and 67% for thermal oils and water, respectively. This reveals that the limitation of the height to width ratio can be different for different types of fluids. The fluid with lower viscosity (thermal oils) can be used at higher height to width ratio of the SPNCL loop than higher viscosity (water), since the mass flow rate becomes constant at higher height to width for lower viscosity fluid (thermal oils) than the higher viscosity fluid (water).

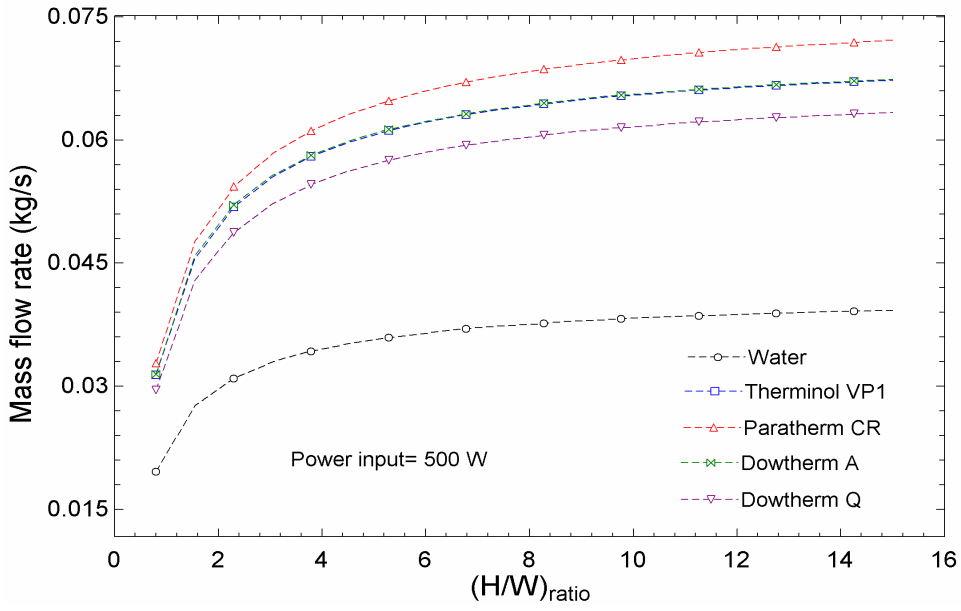

Fig. 3.34 Variation of steady-state mass flow rate with height-to-width ratio for thermal oils.

Figure. 3.35 depicts the effect $(H/W)_{ratio}$ on the effectiveness of water and thermal oils at 500 W input power. The effectiveness decreases with increasing the $(H/W)_{ratio}$ for all the working fluids. It is due to the fact that mass flow rate increases with $(H/W)_{ratio,}$ so the temperature difference between cooler inlet and outlet ($T_{C,in}$-$T_{C,out}$) decreases at a given power. The maximum temperature difference ($T_{C,in}$-T_0) also decreases due to the enhanced heat transfer coefficient (for the increased mass flow rate). Since both the numerator term and denominator terms decrease in the effectiveness equation (3.24), therefore, the net effect on effectiveness depends on the higher rate of decrement.

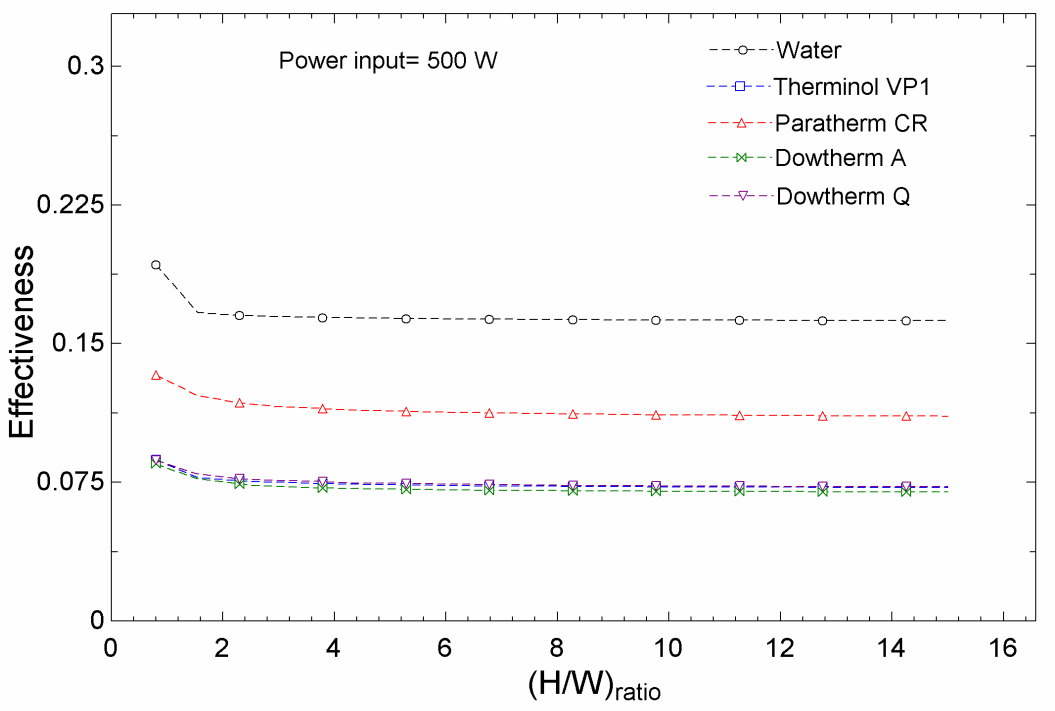

Fig. 3.35 Variation of effectiveness with height-to-width ratio for thermal oils.

Figure. 3.36 depicts the influence of the height-to-width ratio on the total entropy generation rate for water and thermal oil at 500 W input power. The total entropy generation rate declines with the $(H/W)_{ratio}$ due to the decrease in TR value (increased mass flow rate). The pressure drop irreversibility increases with $(H/W)_{ratio}$ due to increases in total loop length and mass flow rate that enhances the entropy generation rate. However, entropy generation as a result of pressure drop is infinitesimal. Henceforth total entropy generation

reduces with $(H/W)_{ratio}$. The entropy generation rate for thermal oils is higher than the water due to lower heat transfer performance.

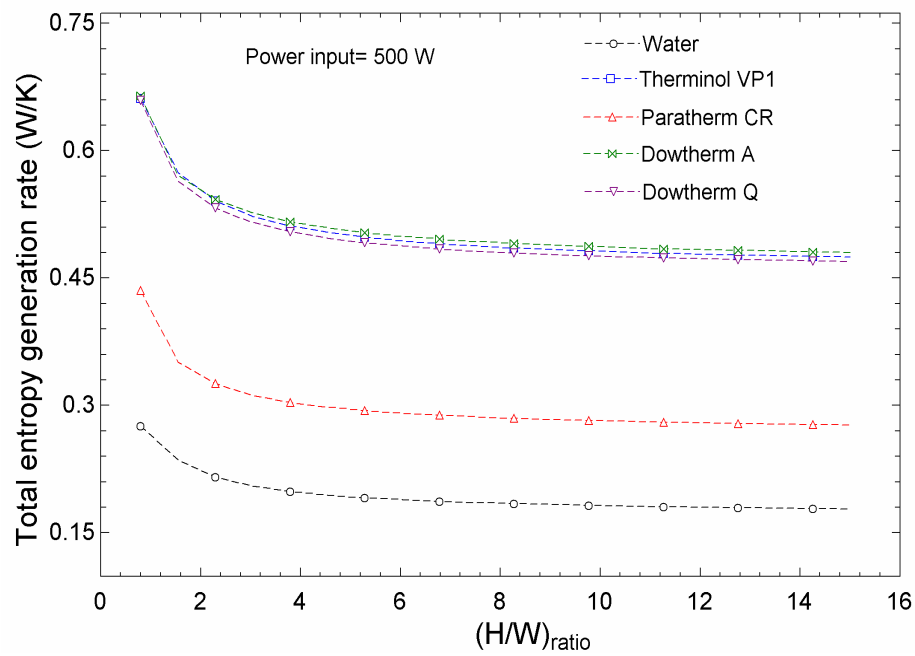

Fig. 3.36 Variation of entropy generation rate with height-to-width ratio for thermal oils.

3.3 Important findings

- The time required to achieve steady-state is less for higher power input. Whereas the steady mass flow rate and total entropy generation increase and effectiveness decreases with increasing power input.
- The shape of the nanoparticle has a very significant effect on the performance of SPNCL; the hybrid nanofluid having CNT and Graphene yields the lowest mass flow rate than others having nanoparticles of spherical shape due to an more increase in viscosity and hence frictional force.
- The mass flow rate and its fluctuation and the time required to achieve the steady-state increase with tube diameter and loop height.
- Both effectiveness and entropy generation increase with decreasing loop diameter and loop height, whereas it increases with increasing loop inclination.

- The binary/ ternary hybrid nanofluids mitigate the instability, which is inferred from the amplitude of mass flow rate oscillations with respect to water in SPNCL.
- At a given power input, the time required to attain steady-state is reduced with binary/ ternary hybrid nanofluids than water. This is definitely beneficial for the system wherein heat removal rate is a major concern and a steady-state is desired.
- Ternary hybrid nanofluids show better performance than binary hybrid nanofluids and base fluids since it has higher effectiveness and a lower total entropy generation.
- Increasing $(H/W)_{ratio}$ decreases the steady-state effectiveness and total entropy generation rate and upsurges the mass flow rate at specified input power.
- The thermal oil shows the early initialization of flow and lower fluctuation of mass flow rate.
- The steady mass flow rate and total entropy generation rate are higher and effectiveness is lower for thermal oils than water.
- Paratherm CR thermal oil shows the best performance compared to all other thermal oils.
- The optimum value of the height to width ratio can be different for different types of fluids.